# FEASIBILITY STUDY OF BASIN STRUCTURE MAPPING USING PASSIVE SEISMIC EXPLORATION TECHNIQUE

## CASE STUDY: AHERO AREA, NYANZA BASIN, KISUMU COUNTY, KENYA

BELCHER MUTISO BONIFACE
I56/67254/2013

Department of Geology
School of Physical Sciences
University of Nairobi

*A dissertation submitted to the Department of Geology in partial fulfilment of the requirements for the degree of Master of Science in Geology of the University of Nairobi*

September, 2015

**Declaration**

I hereby declare that this is my original work and has not been submitted by any other person, form or Institution for any award.

**CANDIDATE:** Belcher Mutiso Boniface (I56/67254/2013)

SIGNATURE: …… DATE: ……..…

This dissertation has been submitted for examination with our approval/knowledge as university supervisors.

**SUPERVISOR:** Prof. Barongo Justus

SIGNATURE: ……..…… DATE: ……..…

**SUPERVISOR:** Dr. Dindi Edwin

SIGNATURE: …… DATE: ……..

**SUPERVISOR:** Dr. Davi Rosalia

SIGNATURE: …… DATE: …….……

**Declaration of Originality Form**

This form must be completed and signed for all works submitted to the University for examination.

**Name of Student**: Belcher Mutiso Boniface

**Registration Number**: I56/67254/2013

**College**: Biological and Physical Sciences

**School**: Physical Sciences

**Department**: Geology

**Course Name**: M.SC. In Geology (Applied Geophysics)

**Title of the work**: FEASIBILITY STUDY OF BASIN STRUCTURE MAPPING USING PASSIVE SEISMIC EXPLORATION TECHNIQUE

CASE STUDY: AHERO AREA, NYANZA BASIN, KISUMU COUNTY, KENYA

**DECLARATION**

1. I understand what Plagiarism is and I am aware of the University's policy in this regard
2. I declare that this thesis is my original work and has not been submitted elsewhere for examination, award of a degree or publication. Where other people's work, or my own work has been used, this has properly been acknowledged and referenced in accordance with the University of Nairobi's requirements.
3. I have not sought or used the services of any professional agencies to produce this work
4. I have not allowed, and shall not allow anyone to copy my work with the intention of passing it off as his/her own work
5. I understand that any false claim in respect of this work shall result in disciplinary action, in accordance with University Plagiarism Policy.

**Signature** _____

**Date** _____

**Acknowledgments**

My sincere gratitude goes to my supervisors/advisors: Prof. Barongo J., Dr Dindi E. and Dr. Davi R. for their guidance, suggestions, corrections and insights which have been of great value in making this thesis a reality. No words can express enough my gratitude to them. Am grateful to the Chairman, Department of Geology-University of Nairobi for the unconditional support throughout the time I was writing this thesis.

I am indebted to Tullow Oil Ltd through the Geophysical Technology and Operations (GT & O) Group and their manager Joe Mongan for sponsoring my fieldwork and data analysis. Others of notable mention from this group are Francesca Martini and John Doherty. Thank you for your efforts towards making this research a success. I have had a lot of support from my former boss, Andrew Skelton and my current line manager Kevin Christopherson championing my being an employee and a student at the same time, I can't thank you enough. Others who have given me tremendous support from Tullow Kenya are Frederic Briens, Greg Smart and Edward Mungatana.

My heartfelt appreciation goes to my family for giving me endless love and hope through the research period even when they had to endure my coming home late in the night from school. They are a priceless gift to me, and am forever indebted to them. Michael Kang'utu, my friend first of all, helped with the fieldwork for this research. Fellow students with whom a serene and friendly environment filled with awesome moments made writing this research easier than it would have been in a different environment.

I cannot exhaust the list of the many people who in one way or the other helped in bringing this research to completion; I will never forget even the smallest of gestures made in making my life easy with this research.

Lastly, all glory to God for giving me strength to pull through. He, indeed, is a faithful God.

**Dedication**

To all men and women who value justice and fairness, and endeavour to make the world a better place than they found it.

**Abstract**

Passive seismic, a non-invasive, cost effective exploration tool, has successfully been used to provide basin structure information in various geological settings. The analysis of ambient vibrations, mainly composed of surface waves, provides velocity structure and depth of a basin. The information obtained through this method can be integrated into analysis of seismic data acquired using the more conventional seismic methods therefore increasing efficiency in oil exploration. In some sensitive area e.g. national parks, archaeological sites and high populated areas, conventional methods may face challenges, therefore a light weight, low impact method may be required to provide basin information in such areas, of which passive seismic technique shows great potential for such an alternative.

This method, however, needs to be tested in a wider variety of more complex geology to assess its reliability in basin architecture mapping. This thesis presents the results of the analysis of passive seismic data, acquired in Ahero area, Nyanza Basin in Kisumu County, Kenya.

The data acquisition was carried out by deploying broadband sensors in single (standalone) stations and in an array configuration in Ahero, Kisumu County in November, 2012 and allowed to record the natural earth vibrations referred to as ambient noise for at least 48 hours. The recorded data was analysed using two techniques-namely horizontal to vertical spectral ratio (HVSR) and frequency wavenumber (F-K)-to yield the main resonance frequency and dispersion curves respectively of the study area. These were then jointly inverted to obtain a velocity model of the basin from which the structure of the basin was deduced.

Velocity profiles obtained from this method highlighted three main velocity contrasts at different depth estimates. The passive seismic results also compared well with results from active seismic; the first two velocity contrasts were located at similar approximate depths although the passive seismic method highlighted a third deeper interface which was not well resolved in the active seismic stacks.

**Table of Contents**

**List of Tables**

**List of Figures**

**Abbreviations and Acronyms**

CDP-Common Depth Point

EARS-East Africa Rift System

FK-Frequency Wavenumber

GPS-Global Positioning System

GT & O- Geophysical Technology and Operations

HVSR-Horizontal to Vertical Spectral Ratio

Hz-Hertz

$V_P$-Compressional wave velocity

$V_S$-Shear wave velocity

1D-One Dimensional

2D-Two Dimensional

3D-Three Dimensional

# CHAPTER 1: INTRODUCTION

## 1.1 Background information

The Kenya Rift region is part of the Eastern branch of the East Africa Rift System that consists of a linear structure extending over 900 km from Turkana basin in the north, to Lake Natron in the south, and splays to form the North Tanzanian Divergence Zone. The Kenya Rift region is divided into four segments: Northern, Central, Southern and Nyanza segments. The recent oil discoveries in Kenya were located in the northern segment and have led to increased exploration interests in the other segments. This research was carried out in the Nyanza segment of the Kenya Rift.

The east-west trending Nyanza half-graben branches from the central Kenyan Rift near Lake Bogoria and disappears westward under Lake Victoria and it is bound by two main faults: the Nyando fault to the north and the Kendu fault to the south. This research was carried out on an area of about ten  square kilometres, of this rift segment around Ahero region in the Kano plains of Kisumu County, about 20km south east of Kisumu City.

A passive seismic method/technique involves the recording of the very low-frequency background ambient seismic wavefield using highly sensitive three-component broadband seismometers (Martini et al., 2013). The seismometers are laid out in the field in arrays of different configurations or stand alone stations depending on the objective of the survey. After a specified recording time, the seismometers, herein also referred to as sensors, are recovered and data are extracted and analysed using various seismic analysis tools.

In this research, two techniques, namely: Horizontal to Vertical Spectral Ratio (HVSR) and Frequency Wavenumber (F-K), were employed in the analysis of ambient vibration wavefields with the aim of determining the thickness of sediments and to derive shallow structural velocity models. These velocity models were used to infer depth of basement through a joint inversion of the outputs of the two techniques following Asten and Henstridge (1984) and Wathelet (2005) suggestions. The dispersion characteristics of surface waves allow the retrieval of the wave velocity as a function of depth. The assumption as pointed out by Wathelet et al. (2004) is that ambient vibrations consist of surface waves, whose dispersion characteristics depend primarily on the body-wave velocities [compressional-wave velocities ($V_P$) and shear-wave velocities ($V_S$)], density and the thickness of the different layers.

### 1.2 Scope of Research

The scope of this research involved three main stages. The first was field work whereby low frequency broadband sensors were deployed in the field in both array configurations and stand alone stations and left to record natural Earth vibrations, referred herein as ambient noise, for at least 48 hours (Martini et al., 2013), that is, to record both day and night data. These were later recovered and data extracted from the instruments for step two of the research. The second step involved data processing and analysis where data was processed and analysed using various geophysical techniques. The final stage was interpretation of the results and report writing.

### 1.3 Literature Review

The use of micro tremors for deriving velocity structures exist for more than twenty (20) years in Japan. Banerji (1924) established a close correlation between variations of seismic ambient noise amplitudes and the Indiana monsoon. Aki (1965) published a note building on this idea to establish the use of microseisms in determining the shallow structure of the Earth's crust while Nogoshi & Igarashi (1970) further developed the use of HVSR of seismic noise to estimate the response of the subsurface structure. Studies carried out by Nakamura (1989) showed that it was possible to establish the predominant frequency (resonance frequency) of a site in both earthquakes and micro tremors through the HVSR calculation. The technique, compared to the conventional seismic methods, was found to be cost effective and highly reliable in showing the relationship between the nature of the topmost sedimentary layers and their fundamental resonance frequencies detected through the ambient noise, with the main focus being to identify the various sedimentary zones capable of amplifying a seismic signal resulting to velocity contrasts (Gu'eguen et al., 2007).

IBS-Von Seht and Wohlenberg (1999), Delgado et al. (2000a) and Parolai et al. (2002) separately published papers on the use of the HVSR technique as a geophysical exploration tool based on the close relationship between fundamental frequency, shear wave velocity and thickness of the soil layer for different sites. Their conclusions for the various sites were that the technique is valid for soils of a few tens of metres thickness to more than 1000 m of thicknesses. Delgado et al. (2000a) also observed that even though the results obtained demonstrated that the method can be useful to gain information about the deep structure of a basin, sources of errors observed in the estimates were due to the simplifications intrinsic to the model, which implied homogeneity in the variability of the shear velocity for the site

investigated. Moreover, the study assumed only two layers of soil (superficial and bedrock) when in fact there were more layers. In addition, the mechanical properties of the soil studied caused some uncertainty in the thickness data used to establish the relationship. The results thus demonstrated that the method was not valid for studying layers which had no marked mechanical contrast between them (high impedance contrasts).

Aki (1957) demonstrated that auto-correlation ratios (dispersion curves) are functions of the phase velocities and of the array aperture. Several other authors carried out studies aimed at improving the results from such arrays e.g. Tokimatsu et al. (1992); and Zhang & Chan (2003). The main assumption in the dispersion curve and HVSR inversion is that, the analysis is based on the fundamental mode of the Rayleigh wave. This assumption is, however, only viable in sites where velocity increases with depth as proposed by Picozzi et al. (2005). Previous studies by Tokimatsu et al. (1992), Zhang & Chan (2003) and Arai (2005) pointed to the necessity of inclusion of higher modes in certain frequency ranges when carrying out the analysis in cases where velocities varied irregularly with depth.

Further studies on joint inversion of the phase velocity dispersion curves and HVSR ratio curves by Parolai et al. (2005) showed that the impedance contrast at the sediment-bedrock interface strongly influences the shape of the HVSR curve around the fundamental frequency. Parolai et al. (2005) successfully carried out a joint inversion of the phase velocity dispersion and HVSR curves putting into consideration the higher modes as they allowed for retrieval of velocity structure details using a genetic algorithm (GA). Genetic algorithms, according to Sambridge and Drijkoningen (1992), are a class of methods that require no derivative information (initial model) and hence avoiding linearization of the problem. They instead rely on random processes to search the model space and find better models. This was consistent with the necessity of a forward model that fitted the phase velocity dispersion and HVSR curves and also taking into account the influence of higher modes. The dependence of velocity on thickness of layers during inversion based on HVSR curves was thus minimised by introduction of the phase velocity dispersion curve in the joint inversion making it possible to determine the characteristics of the S-wave phase velocity and the evaluation of the thickness of the sedimentary layer. Further, the shape and width of the HVSR ratio peak becomes a constraint for the velocity value in the bedrock hence allowing for a reliable evaluation of the impedance contrast (Picozzi et al., 2005). The results obtained with the HVSR spectral ratios are comparable to the transfer function of a site due to the one dimensional (1D) propagation of vertically incident *SH* waves (Lermo and Cha´vez-Garci´a, 1993).

According to Delgado et al. (2000) in equation 1.1, this frequency (f), for a 1D model, is given by:

$$f = {}^{V_S}/_{4Z} \qquad 1.1$$

where $V_S$ is the shear wave velocity in the layer and Z is its thickness. Based on this relationship and assuming f and $V_S$ are known, the thickness of the soil can be determined (Delgado et al., 2000).

### 1.4 Problem Statement

The growing consumption of hydrocarbons especially oil and gas has necessitated more exploration in order to cater for the growing demand. New milestones have been reached in terms of improving exploration and adoption of new techniques. Recently, Tullow Oil Plc, an oil exploration company, incorporated a non-invasive passive seismic technique which utilizes ambient vibrations (also known as ambient noise) to derive velocity contrasts that relate to thickness of sediments (change in lithology) and depth of the basin.

The passive seismic technique has been tested on various geological settings in Kenya, Uganda and Ethiopia where results from other methods (e.g. 2D and 3D seismic, magnetic and gravity) have matched well with the passive seismic results, thus showing great potential for acquiring basin information prior to the more conventional active exploration methods. This information as basin depth would be very useful for decision making on where to focus on with the conventional exploration methods. The passive seismic technique has been demonstrated to be a potential solution to this problem, but it needs more testing in basins of complex geological settings. Such complex conditions are present in the Nyanza basin and provide ideal conditions for the application of this technique. Success of this research would also add valuable information on the applicability of this technique where other methods cannot be employed due to high population density (e.g. Ahero in Kisumu County) or areas of national importance (e.g. game parks). The possibility of integrating and comparing passive seismic and active seismic data for a more detailed result was the ultimate goal of a larger part of this research.

### 1.5 Aim & Objectives

The aim and objectives of this research were:

### 1.5.1 Aim

The aim of the research was to record and analyse low frequency passive seismic data to derive vertical velocity profiles and depth to basement estimates in Ahero region in an effort to compare the retrieved basin depth estimates from this technique with that of 2-D active seismic that had already been carried out in the area.

### 1.5.2 Objectives

The specific objectives of this research were to:

- non-invasively and cost effectively, determine velocity information (velocity profiles) from the resonance frequencies of Ahero.
- establish sedimentary basin thickness and depth estimates, thereby proposing an alternative method for acquiring basin architecture.
- compare passive seismic results with those of the 2D active seismic data.

## 1.6 Justification and Significance of the Research

Passive data analysis offers very significant potential as a cost effective and efficient method for obtaining basin architecture through analysis of its shear-wave velocity information in a wide variety of geological settings. It may be particularly beneficial in inaccessible areas, areas where it is difficult to carry out active seismic surveys due to their importance and sensitivity e.g. archaeological sites, national parks, cities, etc, and in regions where little is known about the basin morphology. This research, therefore, is inspired by the possibility of providing an alternative, reliable and cost effective non-invasive technique to obtain near surface basin information in Ahero region of the Nyanza Basin.

The research is particularly beneficial to the oil industry, the scientific community and policy makers. The rising demand in hydrocarbons justifies the need for better and more effective methods of exploration. Availability of basin structural information prior to more conventional methods of exploration for hydrocarbons can be very beneficial in decision making on which parts of a basin to focus on. This information would also be useful in formulating necessary legislations by providing an in depth understanding of the basin in a given area. The research also aims to equip other researchers with a better understanding of the dispersive characteristics of surface waves and their practical applications to solve geological problems.

# CHAPTER 2: LOCATION, PHYSIOGRAPHY AND GEOLOGY OF THE STUDY AREA

## 2.1 Location and Physiography

Ahero lies in a region of a central plain resulting from deposition after a period of rift faulting, about 20km to the South east of Kisumu City (figures 2.1 and 2.2), forming the Eastern end of the Kano plains. It is bound by latitudes 0° 05' S; 0° 15' S and longitudes 34° 30' E; 35° 00' E. To the north of the study area is the Nyando escarpment standing at 1800m above sea level, to the south is the Nyabondo scarp standing at 1500m and gradually reducing to about 1300m above sea level towards the Homa region. To the west is the Lake Victoria (previously known as the Kavirondo gulf) and the Kericho Tertiary phonolites to the east.

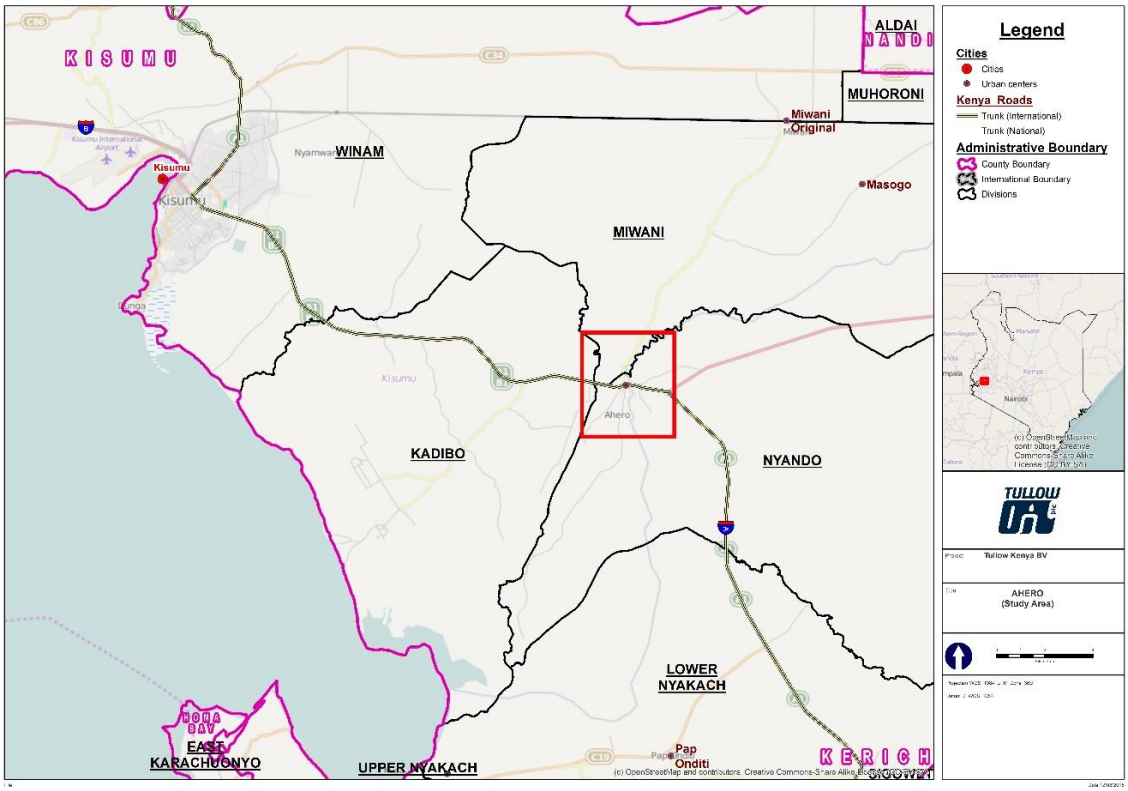


*Figure 2.1: Topographical map of location and administrative boundaries of the study area. Source: Tullow oil Ltd*

This basin is situated between the eastern and western branches of the East African Rift System (EARS) and it covers the northern section of the Tanzanian Craton and parts of the surrounding mobile belts which overlap the edges of the Craton.

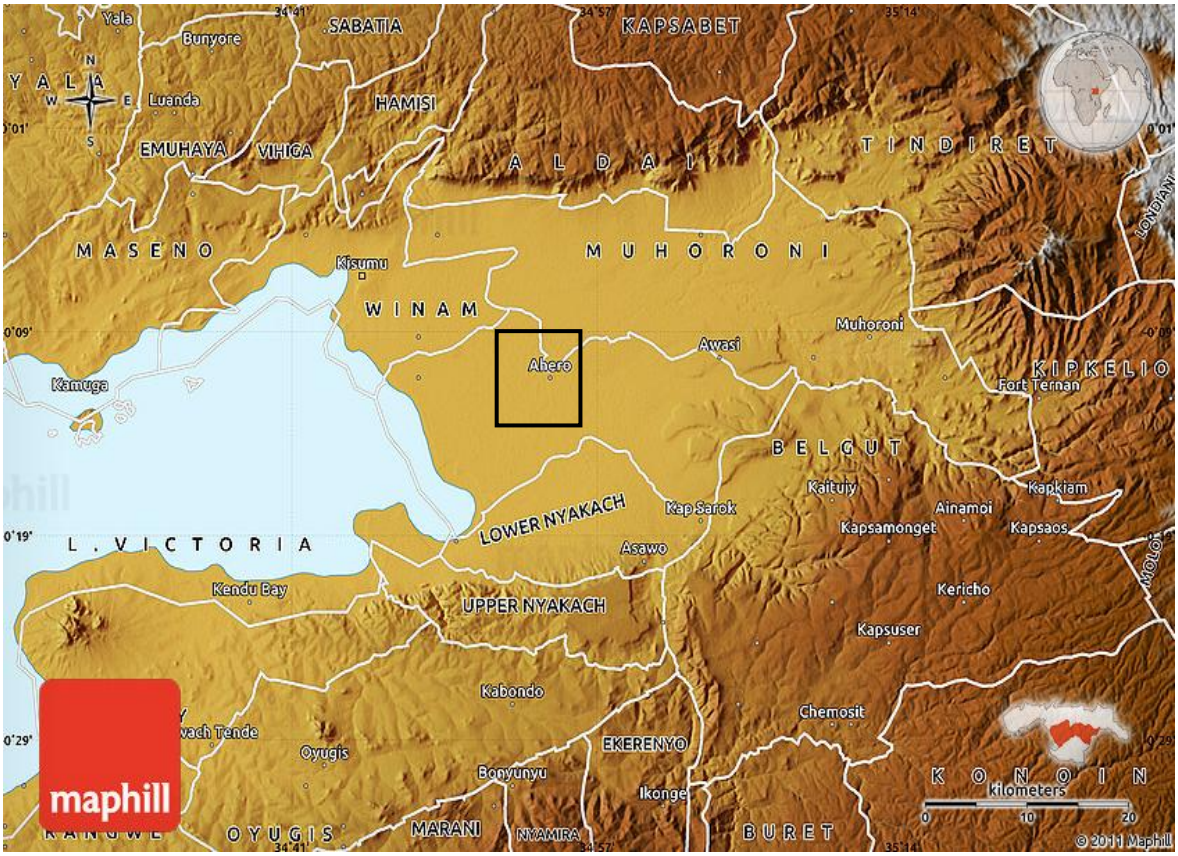


*Figure 2.2: Physiography of study area and its environs presented in a 3-D satellite image. Source: maphill.com*

The drainage pattern generally attains the dendritic drainage pattern with most rivers flowing from east to west. This was probably their direction during the Miocene times according to Saggerson (1952). He further observed that occasional diversion by the phonolites did not always lead to river capture despite the existence of a few cases of river capture in the region.

Faulting and lava flows altered the topography and consequently the drainage of the surrounding sub-Miocene erosion bevel. Saggerson (1952) further observed that the formation of the Kavirondo rift valley led to a new base-level of erosion thus changing direction of drainage of the Nyando scarp to a north-south direction and that of Nyabondo plateau to a south-north direction so that they converged at Nyakach Bay.

### 2.2 Land Use and Land Resources

The land is mainly used for subsistence farming where maize is grown as the main food crop while domestic animals such as goats, sheep, poultry and herds of indigenous cattle are common. The main cash crop in this area is rice, grown in the Ahero rice irrigation scheme although in other regions, e.g., near Kisumu city cotton and sisal are also common. Further to the east is the Muhoroni sugarcane plantation. To the north and north east of the study area

are the Miwani and Chemelil sugar plantations while to the west is the west Kano irrigation scheme.

The major resource in the Kano plains is mainly clays which occur in abundance. These clays are mainly used for building and sculpturing in this region as their calcareous nature is unsuitable for ceramics. Other resources that have been discovered outside the study area include gold mineralization in the Oyugis area to the far south-west and near Ramula to the far north-west of Ahero. Near the Homa mountain is a hill composed entirely of hematite. Magnetite is also common near this mountain although it is not economically viable. Other economic resources include building stone near Kisumu, lateritic ironstone (murram) capping almost all phonolites and limestone quarried at the Homa mountain (Saggerson, 1952).

## 2.3 Geology and Structures

### 2.3.1 Introduction

The area enclosing the Nyanza Basin that lies between the eastern and western branches of the East African Rift System (EARS) has been a locus of deposition since the Precambrian, although the basin has since assumed various configurations with time. The presence of Precambrian through Tertiary volcanic sequences in the western branch of the EARS suggests several episodes of doming in the western branch and subsequent "pondings" of the Nyanza Basin.

The predominant controls on the formation of the Nyanza Basin was tectonic uplifting associated with rifting around the Craton margins, and intersections among a series of north-west trending strike-slip faults which transect the Craton.

### 2.3.2 Geology

The principal rock types of the escarpments enclosing the basin are primarily volcanic rocks. At the edges of the sedimentary basin to the north and to the south, granites and granodiorites are the main rock types while the eastern and north-western edges were dominated by phonolites. The western end of this basin disappears under Lake Victoria, previously known as the Kavirondo Gulf as shown in figure 2.3. Very few outcrops were encountered in the area covered by this research mainly because it lies in the Kano plains which are dominated by sediments. However, the occasional outcrops found have similar characteristics to those of

the ridges surrounding the plains. A geological map summarizing the geology of the study area is shown in figure 2.3 (a more amplified plate is provided in the appendices).

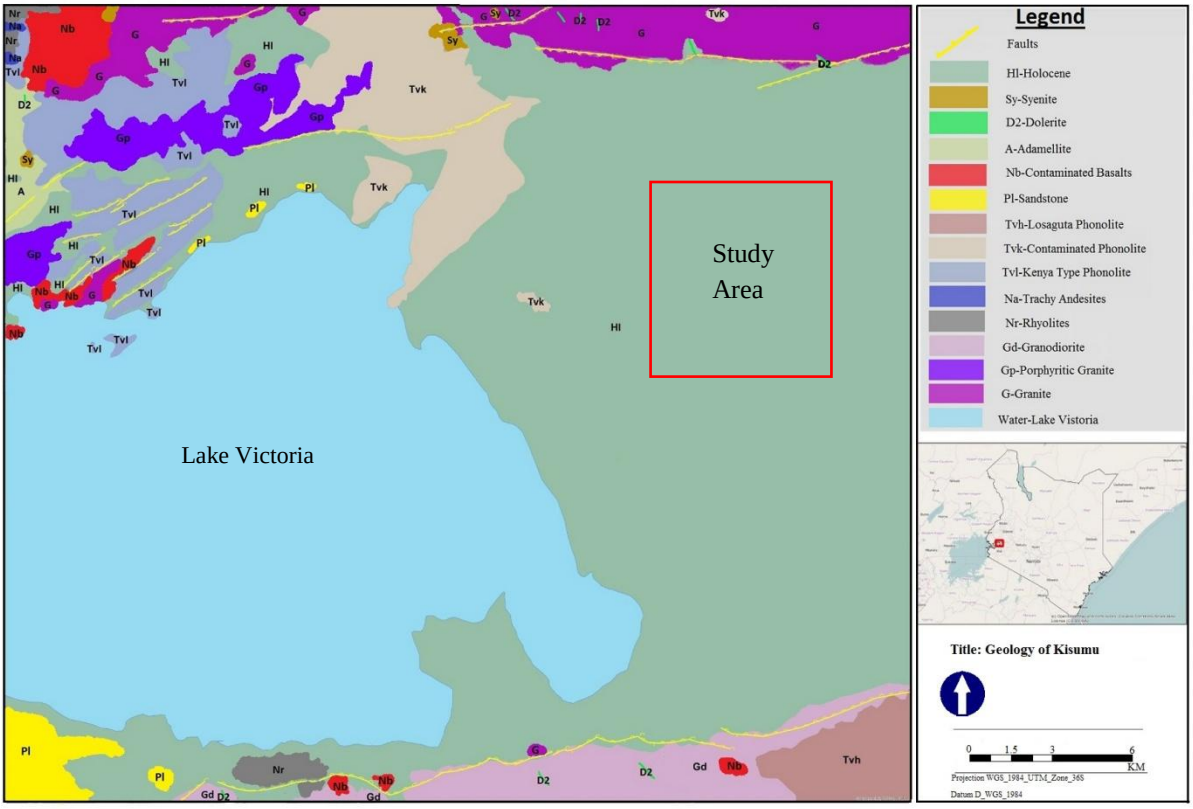


*Figure 2.3: Geological map of Kisumu region. The red box represents the area covered by this research. The yellow lines represent faults in this region. Adopted from Saggerson, (1952)*

### 2.3.2.1 Archean Eon

The oldest rocks in the region are the Archean rocks and are represented mainly by both basic and acidic volcanic namely: granites, granodiorites, basalts, andesites and rhyolites. Also present clastic rocks showing horizons of acid lava overlying the volcanics; characterized by sandstones, quartzites and greywackes. These have, however, been intruded by several episodes of syenitic masses thus resulting into high alteration as observed by Saggerson (1952). Pulfrey (1946) noted that it is impossible to estimate the thickness of the Archean rocks due to the high degree of overfolding associated with the intrusions.

#### 2.3.2.1.1 Granites, Granodiorites and Adamellites

The Archean Eon is mainly made up of both basic and acidic volcanics of the greenstone belt.

Granites and granodiorites form most of the greenstone-trondhjemite-tonalite-granite (TTG) sequence and show a high calc-alkaline affinity (Ichang'i and MacLean, 1991). They are the most dominant rocks along the escarpments enclosing the Nyanza basin; granites are most to the north while granodiorites dominate the southern escarpment. Several episodes of intrusions by syenitic masses and adamellites have resulted in granites of different degrees of alterations and are isoclinally folded about axes that have a east-westerly trend (Ichang'i and MacLean, 1991; Salop, 1983).

In some parts, the volcanics are unconformably overlain by clastic rocks of almost similar age represented by sandstones and greywackes and show well developed graded bedding typical of turbidites and are as well isoclinally folded.

#### 2.3.2.1.2 Basalts

Most of the basic volcanics are dominated by tholeiitic mafic basalts that were erupted into a submarine environment. Outcrops to the north-west show minimal alteration and thin sections carried out by Saggerson (1952), their basaltic nature is recognizable. They are dense, fine grained and black-blue to grey-green in colour and break in a splintery, conchoidal fracture as observed by Saggerson (1952). Under the microscope, he established that the most dominant dark mineral in the basalts is the prismatic hornblende which occurs as micro-phenocrysts or small fibrous laths or needles in the matrix. Chlorites and epidote occur as secondary minerals.

The basalts to the south-west show low-grade schistose characteristics and high degrees of alteration under the microscope. The main minerals in these rocks are calcite, epidote, chlorite, albite, hornblende, actinolite and quartz (Saggerson, 1952). Presence of the montmorillonite clay minerals in the Kano plains sediments suggests that the basalts weather to smectite group of clay minerals under humid conditions hence the resultant of the black to grey alluvium covering the plains; often known as black cotton soils.

#### 2.3.2.1.3 Rhyolites and Andesites

Both of these rock formations occurred further away from Ahero in Kendu, Oyugis and Kabondo. Although they may not directly influence the geology of the study area, they may have contributed to the formation of sediments in the basin. Patches of these rhyolites were occasionally found in major outcrops of the Archean rocks while andesites were mainly seen in regions dominated by the granites.

#### 2.3.2.2 The Proterozoic Eon (Kisii Series)

The Kisii series occurs further to the south of Nyabondo scarp, and unconformably overlies the Archean greenstone belts. Saggerson (1952) observed that the series is dominated by porphyritic and course-grained basalt group at Mkaye predominantly dipping 30° and 34° in a south-easterly direction; whereas dips of 20° are dominant in the quartzite band to the west of the Kisii series outcrop as a result of faulting in this region.

Saggerson (1952) described the texture of these rocks as being generally intersertal although seriate hyalopilitic and vitrophyric textures are also common. The groundmass is often glassy and tends to be spherulitic with "comb" structures.

Non-porphyritic basalts are also common in the outcrop. These are characterized by dense, non-porphyritic, vesicular, well-jointed, splittery basalt flows dipping in a south to south-east direction. Their textures vary considerably, with hyalopilitic being the main texture. Other rock types in this series that are not dominant are quartzites, cherts and porphyritic and porphyritic felsites.

#### 2.3.2.3 Neogene Period

##### 2.3.2.3.1 Miocene Sediments Epoch

The deposition of the Miocene sediments is speculated to have taken place probably in a lake or lakes on the sub-Miocene peneplain, represented by the pre-Rata phonolites surface on which Mariwa deposit lies (Saggerson, 1952). These sediments were buried by lava outpourings followed by rift faulting. Post-Neogene erosion has, however, washed out the major fault scarps and re-excavated these deposits. Fossils collected from the re-exposed sediments suggest their age to be Lower Miocene as observed by Saggerson (1952). Kent (1944) after examining a number of fossil mammals, reptiles and other animal remains collected from these beds postulated that these fossils seemed to be as old as the beds themselves and not derived from older beds.

Others are grey-yellow to green tuffs which are occasionally banded with thin layers of mudstone veined and welded by calcite occurring near Homa Bay. Unidentifiable plant remains are prominent in these tuffs and could be inferred to being of a probable Miocene forest overlain by the tuffs and agglomerates which were later buried by the phonolites.

##### 2.3.2.3.2 Neogene Volcanics

Neogene lavas are dominantly phonolites and are most dominant in the north of the Kavirondo gulf and a few outcrops to the south around Nyabondo and Homa. These are mostly related to the Pleistocene faults and might have been fissure eruptions preceding the movement that would later result into fault lines during the phases of domal uplift in the Plio-Pleistocene times. The phonolites are distinctly of three types namely: Kenya type, the Losaguta type and the Kericho type further to the east of Ahero outside the map (Saggerson, 1952.

#### 2.3.2.4 Quaternary Period

##### 2.3.2.4.1 Pleistocene Epoch

Deposits of this age are dominant in this area and are mostly lacustrine sediments of different lithologies and compositions to the east of the Kavirondo Gulf. They vary from gravels to mudstones derived directly, by erosion, from neighbouring rock formations. Saggerson (1952) observed that borehole data from a well in Kisumu indicated depths of up to 18m of lake sediments while another borehole in Miwani showed depths of up to 138m of lacustrine sediments. The sediments were deposited in four different pluvial periods where deposition occurred followed by gentle folding and faulting due to eruption of the Homa mountain volcano during the first pluvial period. This was followed by a period of tilting towards the west. The third pluvial period saw further deposition, faulting and folding take place followed by erosion. The fourth pluvial period was a period of deposition free from faulting and folding (Saggerson, 1952).

#### 2.3.2.5 Holocene Deposits Epoch

Generally the region is covered by hill wash, gravels, soils, alluvial flats clay deposits and sands. The Kano plains region is predominantly covered by black cotton soils and with only small areas along the ridges dominated by hill wash. The clays are calcareous and vary from black to grey in colour. They are poorly drained and are mostly composed of montmorillonite minerals.

### 2.3.3 Structures

#### 2.3.3.1 Introduction

The main geological structures of interest in the area of study are faults. The Kavirondo gulf and the Kano plains sit on a central graben (regions that lie between normal faults and are

either above or lower than the area beyond the faults) bound by the Kavirondo rift faults as shown in figure 2.5.

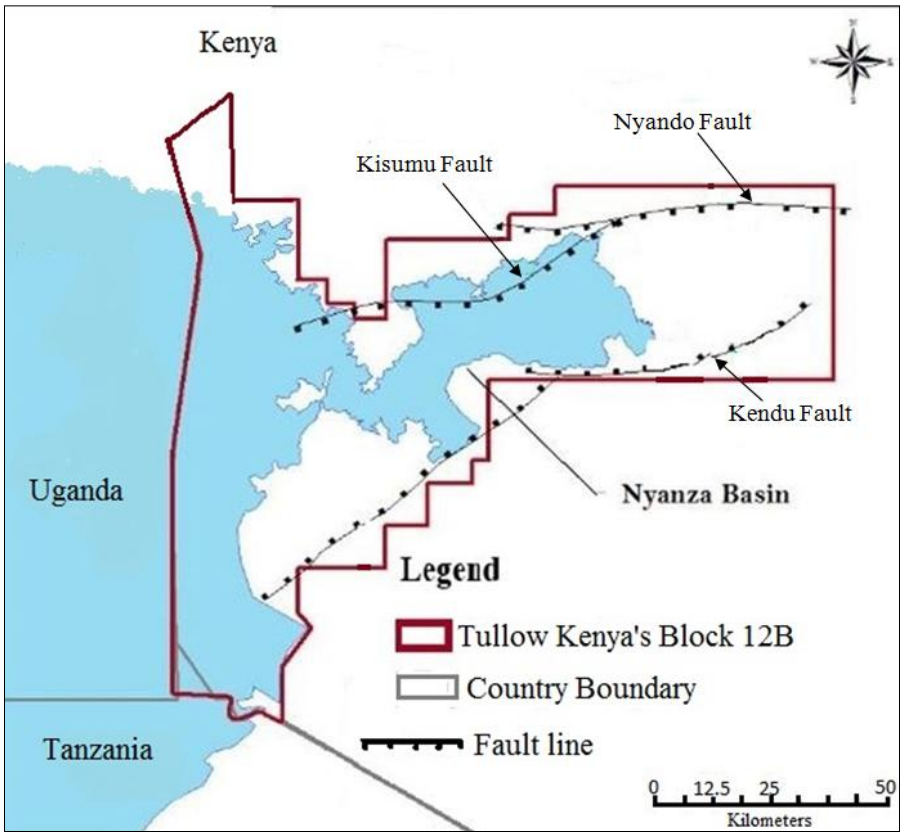


*Figure 2.4: Structural map of Nyanza Basin. Adopted from Swala Energy Ltd*

According to Saggerson (1952), the Lower Miocene trough was probably bound by faults of no great magnitude aligned in the east-west direction and later rejuvenated in the form of Nyando, Kendu, Kibos and Kisian faults, forming the graben as seen today.

#### 2.3.3.2 Nyando and Kendu Faults

The Nyando and Kendu faults are the most dominant faults in the study area running in the east-west trend bounding the basin to the north and to the south respectively.

The Nyando fault runs from Kibos to Miwani and it is estimated to be about 19km long. According to Saggerson (1952), it was responsible for the formation of the Nyando escarpment. Although the fault is not visible due to the possibility of having been covered by alluvium, truncated spurs are still visible as evidence of a fault but no evidence of shearing associated with this fault has been found.

Kendu fault, on the other hand, is estimated to be about 37km in length and with no fault scarp behind it. Evidence of shearing and epidotization has also been observed in the

intrusives cut by the fault with the most evident shear zone of about 100m wide found near Kendu.

#### 2.3.3.3 Kisumu Faults

These are three parallel faults trending north-east to south-west and are responsible for the scarp near Kisumu Township. Saggerson (1952) observed that the three faults formed a zone cutting the Nyando and Kisian faults causing a movement of the two blocks relative to each other. The Nyando block was seen to have moved north-wards while the Kisian block moved to the south.

# CHAPTER 3: BASIC PRINCIPLES OF SEISMIC SURFACE WAVES AND THEORY OF PASSIVE SEISMIC TECHNIQUE

## 3.1 Introduction

Seismic waves are vibrations or shockwaves of released energy propagating through the Earth. They are generated by sudden breaking of rocks as a result of movements of the Earth's tectonic plates, but may also be caused by explosions, volcanoes and landslides. There are two main types of seismic waves classified according to their propagation properties. These include body waves and surface waves. The seismic wavefield is also composed of persistent ground vibrations of low frequency known as the ambient wavefield or ambient vibrations, commonly known as 'ambient noise.' These are discussed individually as follows.

### 3.1.1 Body waves

Body waves travel through the body of the Earth. As the waves travel through different densities and stiffness, they can be reflected and refracted. They are of two types: longitudinal waves and transverse waves.

#### 3.1.1.1 Longitudinal waves

Longitudinal waves are also known, in seismology, as primary (P) waves because they are the fastest of all seismic waves. They travel in a push and pull motion in the direction of propagation (figure 3.1). The material they propagate through oscillates in compressions and expansions. They are, therefore, also known as compressional waves.

P-waves temporarily change the volume of the material they travel through and propagate in both solids, liquids and in gases. Other terminologies used to describe these waves are pressure and dilational or irrotational waves.

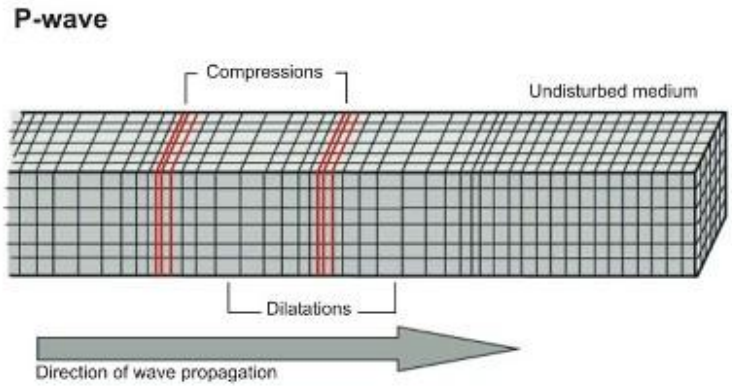


*Figure 3.1: Compressions and dilations of a propagating longitudinal wave in the direction of particle motion. (Adopted from Bolt, 1978)*

#### 3.1.1.2 Transverse waves

Transverse waves, also referred to as secondary or shear (S) waves, propagate by shearing and rotating of the medium (figure 3.2). The particle motion is perpendicular to the direction of particle motion.

S-waves do not alter the volume of the medium but can change its shape. They propagate in solids but not in liquids and gases.

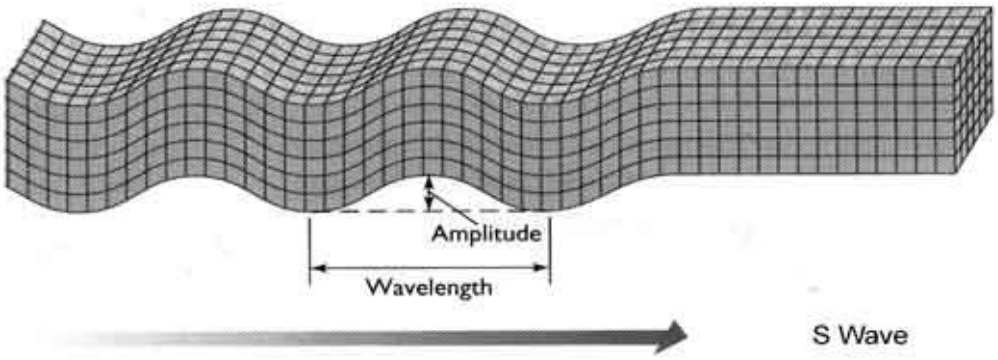


*Figure 3.2: Propagation of elastic transverse waves perpendicular to the direction of particle motion. (Adopted from Bolt, 1978)*

### 3.1.2 Surface waves

These are elastic waves that travel along or parallel to the Earth's surface. They have larger amplitudes, longer wavelengths and are slower than body waves. They are said to originate from the condition of vanishing stress at a boundary of a domain and are characterized by a much lower rate of geometric attenuation than body waves (Foti, 2014). They are of two types: Love waves and Rayleigh waves.

### 3.1.2.1 Love waves

The particle motion of these waves is horizontal and perpendicular to the direction of propagation. They cause shape changes in the medium they travel through and are generally responsible for the horizontal shifting associated with earthquakes. They are generally faster than Rayleigh waves and attenuate faster with depth (Novotny et al., 1996). Their velocity depends on frequency (Nogoshi and Igarashi, 1970).

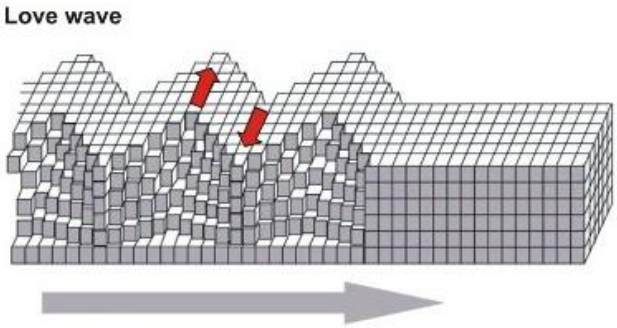


*Figure 3.3: Propagation of Love waves is horizontal and parallel to surface as shown by the red arrows. (Adopted from Bolt, 1978)*

### 3.1.2.2 Rayleigh waves

Rayleigh waves propagate in both transversal and longitudinal motions. Their amplitude exponentially decays with depth. The particle oscillates in a retrograde elliptical motion (figure 3.4), in the vertical plane and parallel to the direction of propagation (Novotny et al., 1996). Rayleigh wave, like Love waves, velocity depends on the frequency of the particle motion, thus they are said to be dispersive (Nogoshi and Igarashi, 1970). These characteristics make them ideal for site characterization. Xia et al. (2003), showed that Rayleigh waves are strongly dependent on S-wave velocity while weakly dependent on the P-wave velocities, density of the medium and the thickness of the soil layers.

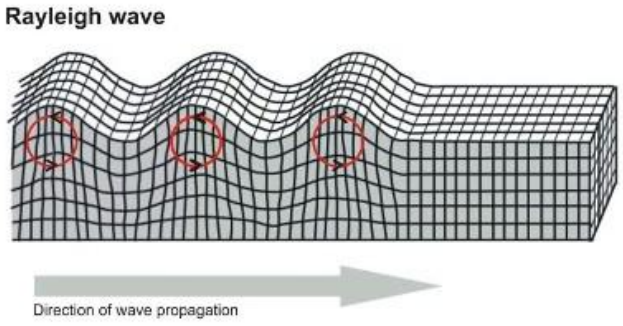


*Figure 3.4: Propagation of Rayleigh waves. (Adopted from Bolt, 1978)*

Inversion of Rayleigh wave fundamental mode gives a robust and reliable estimation of the shear wave velocities from which depth estimates of a site can be obtained (Wathelet, 2004; and Yilmaz, 2015).

### 3.1.3 Ambient Wavefield (Ambient 'noise')

Ambient seismic wavefield, often called seismic 'noise' is the generic term used to denote ambient ground vibrations of natural and anthropogenic origins. The low frequency part of the spectrum, usually below 1Hz, is mainly generated by natural causes, e.g., ocean waves and is generally defined as microseisms. Around a frequency of 1Hz, the waves are mainly caused by local sources such as wind and other meteoric conditions. Above 1Hz ambient vibrations are generated by human activities and machinery and are known as microtremors (Bonnefoy-Claudet et al., 2006).

The ambient wavefield is predominantly composed of surface waves (section 3.1.2) although a small proportion of body waves is also present (Bonnefoy-Claudet, 2006). The surface waves are dispersive, i.e., their phase velocity (V) varies with frequency. This dispersive property makes them ideal for basin depth mapping. The relationship between shear wave velocity and depth can be explained by plotting a dispersion curve (figure 3.5) which shows that phase velocity (often plotted as slowness-the inverse of phase velocity) is a function of frequency (Foti, 2000).

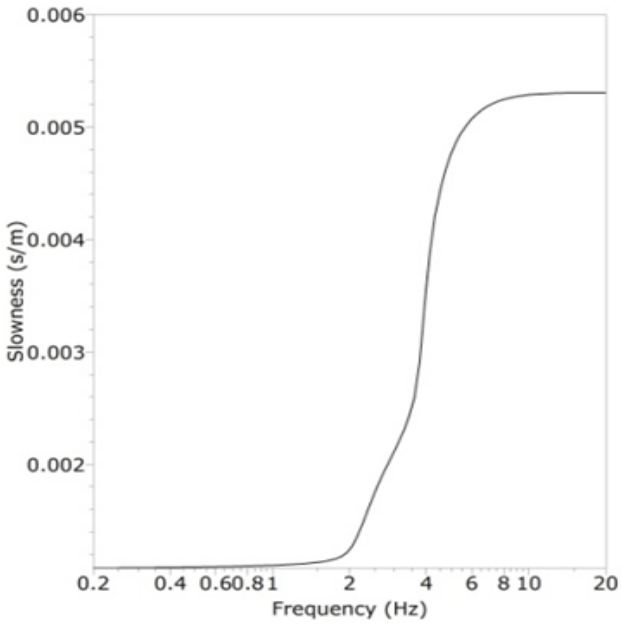


*Figure 3.5: Example of a dispersion curve. Slowness (inverse of phase velocity) decreases with increase in frequency.*

Inversion of Rayleigh wave fundamental mode gives a robust and reliable estimation of the shear wave velocities from which depth estimates of the site can be obtained (Wathelet, 2004; and Yilmaz, 2015).

### 3.1.4 Rayleigh wave geometric dispersion

In a homogenous, isotropic, linear elastic half-space, Rayleigh waves are not dispersive and, therefore, their propagation is dependent on the medium's mechanical properties and not on frequency. However, in a heterogeneous medium, the geometric dispersion phenomenon arises causing the phase velocity of the waves to be dependent on frequency (Foti, 2000).

Foti et al. (2014), suggests that energy associated with Rayleigh wave motion is confined within a depth of one wavelength (λ) from the free boundary causing Rayleigh waves with long wavelengths to penetrate deeper into the medium than those with short wavelengths. In terms of frequency, it can be thus said that high frequency waves are confined to shallow depths whereas low frequency waves are associated with deeper depth penetration as shown in figure 3.6 (Foti et al., 2014). In this figure, both high frequency and low frequency particle motions in a heterogeneous layered medium are illustrated.

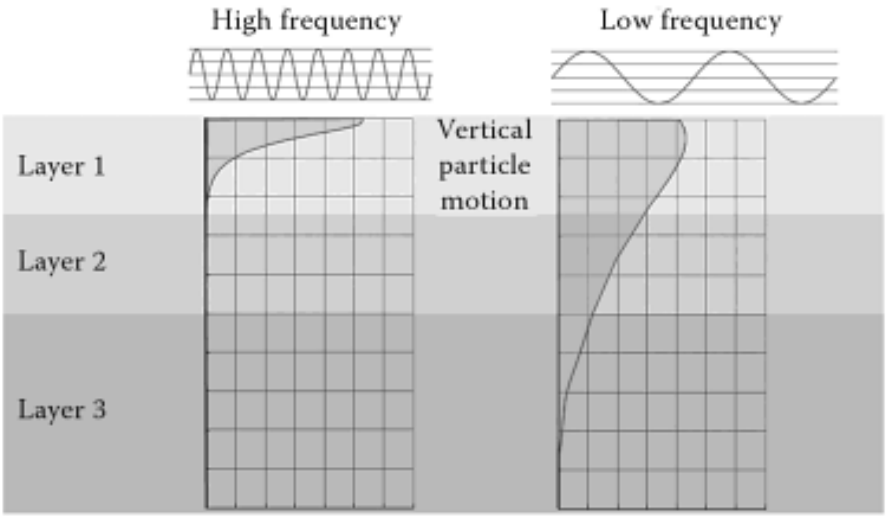


*Figure 3.6: Dispersion of Rayleigh waves in layered medium. Adopted from Foti et al. (2014)*

Mathematically, according to Foti (2000) in equation 3.1, the relationship between wavelength and frequency can be represented as:

$$\lambda_R = \frac{V_R}{f} \qquad 3.1$$

where:

$\lambda_R$ is the Rayleigh wave wavelength,

f is the frequency of the wave,

$V_R$ is the phase velocity- a function of the frequency (Foti, 2000).

Group velocity (U) is another property caused by the dispersive behaviour of surface waves. This is the velocity of the pulse of energy (envelop) and can be shown to consist of multiple single frequency signals travelling at different velocities due to dispersion (Foti, 2000). It is shown in figure 3.6 that the phase velocity (carrier) travels faster than the group velocity (envelop) for normally dispersive profiles (where V is greater than U). For non-dispersive medium, the group velocity and phase velocity coincide (Foti, 2000).

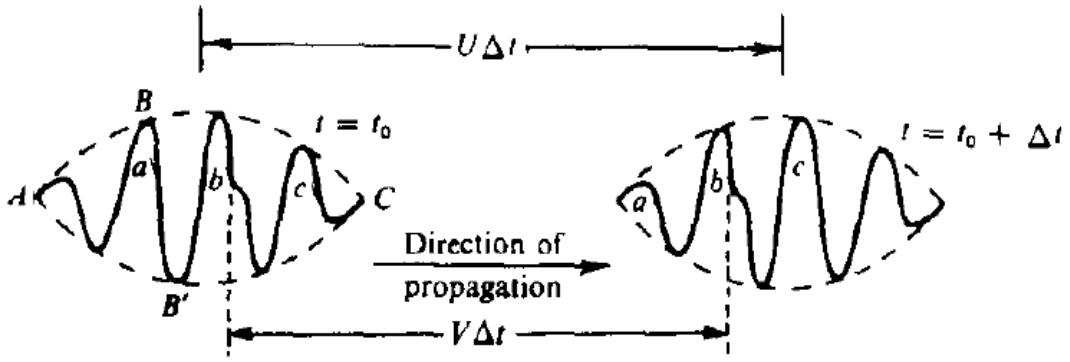


*Figure 3.7: Relationship between group velocity and phase velocity of Rayleigh waves. Adopted from Foti (2000)*

Group velocity is recorded at the surface by sensors and is responsible for the differences in arrival times of the waves at the array stations (figure 3.7) depending on the dispersive characteristics of the medium through which they propagate.

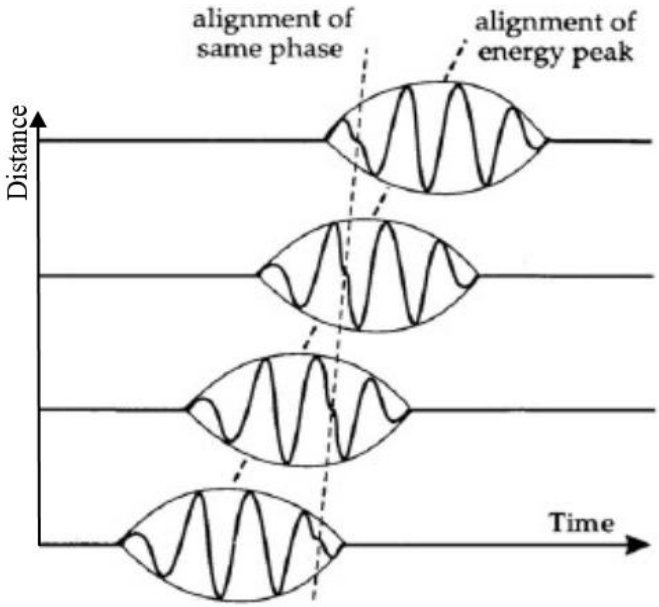


*Figure 3.8: Group velocity arrival at different sensors. Adopted from Foti, (2000)*

From equation 3.2 (Foti, 2000), the relationship between group and phase velocities is given by:

$$V_g = \frac{\delta\omega}{\delta k} = V_p - \lambda \frac{\delta V_P}{\delta\lambda} \qquad 3.2$$

where:

$V_g$ is the group velocity,

$V_p$ is the phase velocity,

$\omega$ is the dispersion relation and indicates the dispersion properties of a medium.

From this equation, it can be seen that:

If $V_g = V_p$ the medium is said to be none-dispersive (phase velocity does not depend on the wavelength of the propagating wave).

If $V_g < V_p$ the medium has normal dispersion

If $V_g > V_p$, the medium has anomalous/inverse dispersion (Foti, 2000).

A summary of S-wave phase velocities through different rock types is attached (table 3.1) which are closely related (Foti, 2000; and Wathelet, 2005) to the velocities of Rayleigh waves. These velocities are, however, subjective and could change with various conditions in the same rock formation, e.g., fracturing.

*Table 3.1: S-wave velocities (m/s) and their corresponding P-wave velocities through different rock formations. Source: Adopted from Stanford Rock Physics Laboratory – Bourbié (1987)*

| **Types of formation** | **P wave velocity (m/s)** | **S wave velocity (m/s)** | **Density ($g/cm^3$)** |
|---|---|---|---|
| Scree, Vegetal soil | 300-700 | 100-300 | 1.7-2.4 |
| Dry sands | 400-1200 | 100-500 | 1.5-1.7 |
| Wet sands | 1500-2000 | 400-600 | 1.9-2.1 |
| saturated shales and clays | 1100-2500 | 200-800 | 2.0-2.4 |
| Marls | 2000-3000 | 750-1500 | 2.1-2.6 |
| Saturated shale and sand sections | 1500-2200 | 500-750 | 2.1-2.4 |
| Porous and saturated sandstones | 2000-3500 | 800-1800 | 2.1-2.4 |
| Limestones | 3500-6000 | 2000-3300 | 2.4-2.7 |
| Chalk | 2300-2600 | 1100-1300 | 1.8-3.1 |
| Salt | 4500-5500 | 2500-3100 | 2.1-2.3 |
| Anhydrite | 4000-5500 | 2200-3100 | 2.9-3.0 |
| Dolomite | 3500-6500 | 1900-3600 | 2.5-2.9 |
| Granite | 4500-6000 | 2500-3600 | 2.5-2.7 |
| Basalt | 5000-6000 | 2800-3400 | 2.7-3.1 |
| Gneiss | 4400-5200 | 2700-3200 | 2.5-2.7 |

Rayleigh waves exhibit a second property that can be used to constrain local ground structure called ellipticity. Ellipticity is the ratio between the horizontal and vertical axes of the particle motion. It is linked to the underground structure and also complementary to the dispersion curve (Hobiger et al., 2012). The spectral ratio of the horizontal to vertical components yields a singular peak corresponding to the resonance frequency of that site. According to Hobiger et al. (2012), the resonance frequency peak of a site with a shear-wave impedance contrast between overlying sediments and the bedrock corresponds to the Rayleigh wave ellipticity curve.

### 3.1.5 Frequency Wavenumber

Generally, the basis of most signal analysis techniques is data mapping from one domain to another domain by use of Discrete Fourier Transform. For example, most signal analysis techniques involve data mapping from a time domain to a frequency domain and then to the wavenumber domain (in space). The application of these independent variables (time and

space) is the basis of the double transform, that is, it results from the two successive applications of the 1D transform: the first application in time taking the raw data from the time domain (tx) to the frequency domain (fx) and a second application in the spatial direction yielding the frequency wavenumber domain (fk), (Foti, 2000).

In this research, only a 1D transform was employed for array data analysis in that, raw data was mapped from the frequency domain (fx) to the frequency wavenumber domain (fk). Simultaneous waveform recordings of a group of spatially distributed stations (array) were analysed in many narrow frequency bands for individual analysis windows cut from the overall recordings. In every analysis window and frequency band, a grid search was performed in the wavenumber domain to obtain the propagation properties of the most coherent plane wave arrivals in the analysis window (geopsy.org, 2008). The main assumption of this method is that horizontal plane waves travel across the array. Considering a wave with frequency f, a direction of propagation ($k_x$ and $k_y$) and a velocity (or wavenumbers along x and y horizontal axis), the relative arrival times can be calculated at all sensor locations and phases shifted according to their respective time delays (Wathelet, 2005). Summation of the shifted signals in the frequency domain gives the array output. Dividing the array output by the spectral power yields semblance (quantitative measure of the seismic data coherency recorded from multiple channels that is equal to the energy of a stacked trace divided by the energy of all the traces making up the stack) according to Asten and Henstridge (1984). If the waves travel in a given direction and at a given velocity, all the array sensor contributions will stack constructively hence resulting in a high array output. According to Wathelet (2005), locating the maximum semblance in the plane ($k_x$, $k_y$) gives an estimate of the azimuth and the velocity of the waves across the array.

### 3.1.6 Array Response

The resolution capabilities of an array can be summarized by the shape of its beam pattern known as the array response function. It is also called the array transfer function because the array output is the convolution of the wavefield and the theoretical frequency wavenumber response (Wathelet, 2005). The resolving power of an array (or capability to distinguish between two similar signals) strongly depends on the number of receivers used for the survey and the geometry of the array. Theoretically, the frequency wavenumber response of an array is given as a semblance map. According to Wathelet (2000) in equation 3.3, for a single

vertically incident plane wave ($k_x$, $k_y$) equal to (0, 0), the array response (AR) in this plane is given by:

$$AR(k_x, k_y) = \frac{1}{n^2} \left| \sum_{i=1}^{n} e^{-j(k_x x_i + k_y y_i)} \right|^2 \quad 3.3$$

where n is the number of sensors in the array and ($x_i$,$y_i$) are their coordinates. This equation (Adopted from Wathelet, 2005) shows that, below the theoretical aliasing wavenumber, the position of the highest peak of the array is linked directly to the azimuth and the apparent velocity of the propagating wave. According to Wathelet (2005), aliasing in more complex wavefields may occur due to summation of the lateral peaks from contributing waves of array transfer function. The two most important parameters directly related to array geometry are the minimum wavenumber ($k_{min}$) responsible for the array resolution power limit and the maximum wavenumber ($k_{max}$) responsible for controlling aliasing limits as shown by equations 3.4 and 3.5. From Wathelet (2005), they are defined as follows:

$$k_{min} = {}^{2\pi}/_{D_{max}} \quad 3.4$$

$$k_{max} = {}^{2\pi}/_{D_{min}} \quad 3.5$$

where $D_{max}$ is the maximum interstation distance, called the array aperture (defined by the array diameter), and $D_{min}$ is the minimum interstation distance. The dispersion curve obtained from array processing is considered to be reliable within these two boundaries.

### 3.1.7 Inverse Problem

An inverse problem is the mathematical process of predicting (or estimating) the numerical values of a set of model parameters of an assumed model based on a set of data or observations. This can be summarized as shown in figure 3.8.

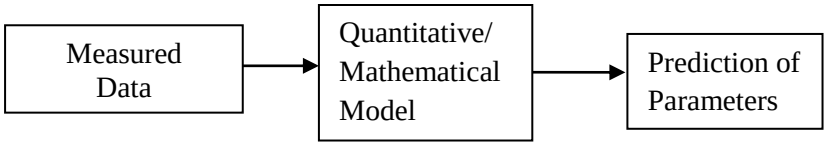


*Figure 3.9: A diagrammatic illustration of an inverse problem. (Modified from Menke, 1989)*

There are different available methods of inversion, but due to non-uniqueness of the inverse problem, i.e., it has an infinite number of solutions, each with a different combination of null

vectors, the Neighbourhood Algorithm was preferred over other classical linearization methods.

The neighbourhood method is a direct search method which allowed the whole parameter space to be investigated (Wathelet, 2005), based on the partition of the Voronoi cells (figure 3.9) as was proposed by Sambridge (1999a). According to Wathelet (2005), it involves sampling all the regions of the parameter space where models with acceptable data fit are found.

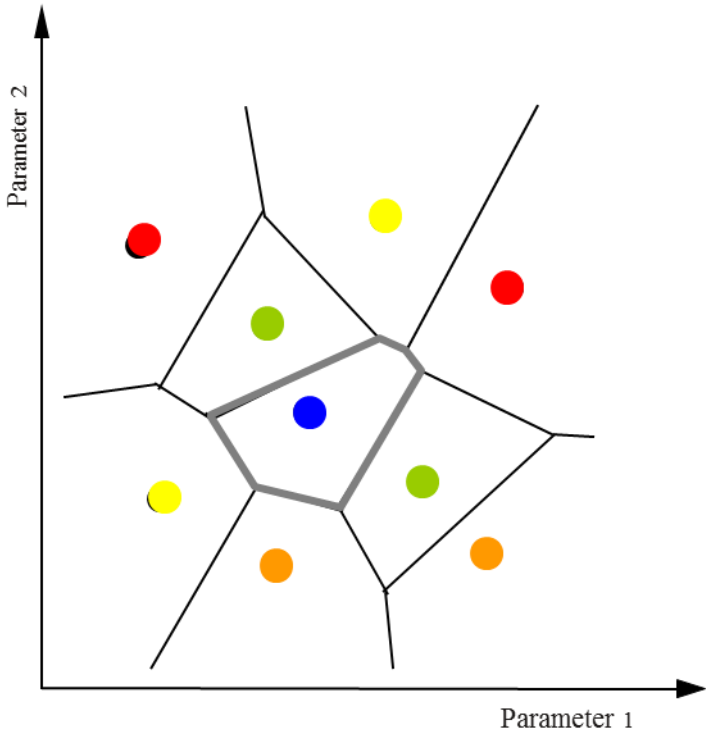


*Figure 3.10: Models in Voronoi cells (multicolour dots). The lines show the limits of cells. Adopted from Wathelet (2005)*

The Voronoi decomposition of the parameter space is the basis of the misfit function approximation, progressively refined during the inversion process (Wathelet, 2005), as shown in figure 3.10 where the grey cell shows lowest misfit. In this case, the approximation was set as a constant inside each cell in the processing software, GEOPSY, (geopsy.org, 2008) and misfit value calculated from the centre outwards for each cell as shown in figure 3.10 (Wathelet, 2005).

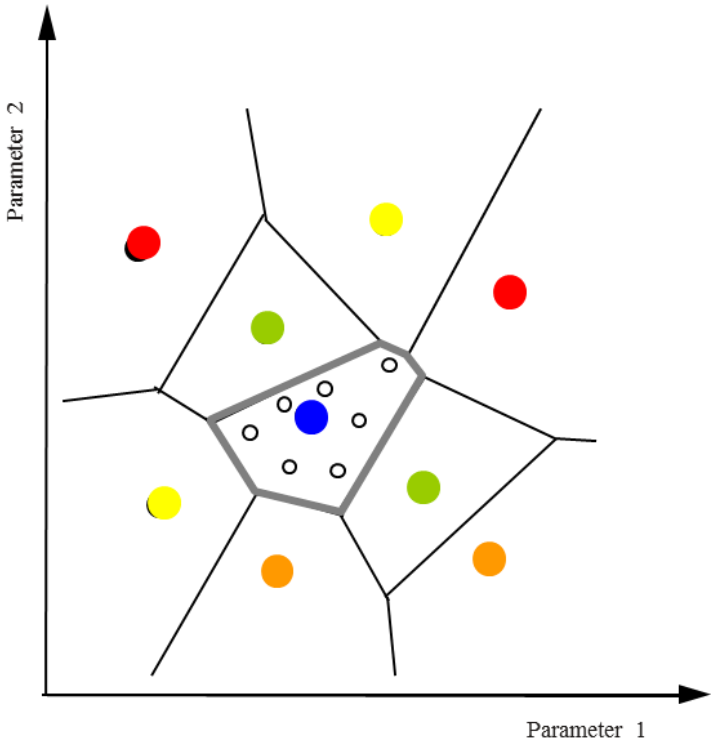


*Figure 3.11: A two dimensional parameter space. The grey cell shows lowest misfit. Seven more models are created within this cell. Adopted from Wathelet (2005)*

After each iteration, the size of the original cell decreases as the sampling rate increases. If, for example, the cell with the grey outline has the lowest misfit, the density of sampling will not decrease systematically after each iteration as shown in figure 3.11. This is an interesting property of the Voronoi geometry which allows the centre of sampling to jump from place to place, whilst always sampling the most promising cells with lowest misfit (best cells) regions simultaneously (Wathelet, 2005).

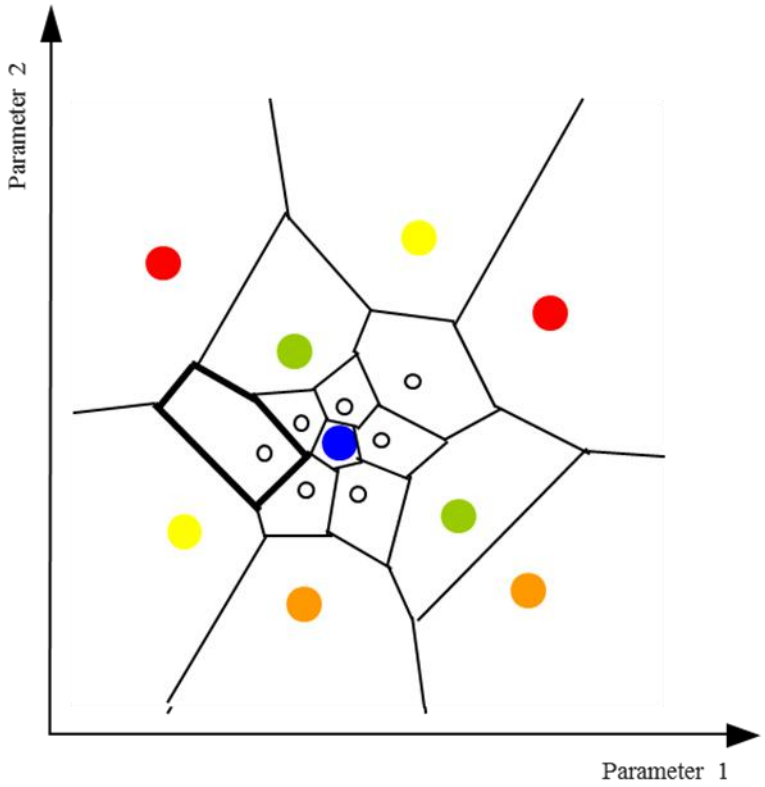


*Figure 3.12: After first iteration, the size of the cell decreases with increase in sampling. Adopted from Wathelet (2005)*

Surface waves are dispersive in nature, e.g. their velocity ($V_s$) varies as a function of frequency, which, in turn, controls their penetration depth (Aki and Richards, 2002). The dispersive property was utilized in this research to derive the shear-wave velocity ($V_s$) versus depth through an inversion process as proposed by Wathelet et al. (2004). Model properties of dispersion curves, as observed by Wathelet (2005), vary only with depth (1D structure), and thus profiles are discretized along the vertical axis only. The parameters that characterized each layer in the inversion process for this research were mainly the compression-wave velocity ($V_P$), the shear-wave velocity ($V_s$), the density ($\rho$) and thickness.

Of these, the most influential is the shear-wave velocity ($V_s$) with varying velocities through different layers. Reynolds (1997) and Xia et al., (2003) observed that this velocity reach up to about three thousand five hundred metres per second (3500 m/s) in hard basement rock. The compression-wave velocity ($V_P$), as postulated by Wathelet (2005), has very minimal influence on Rayleigh-dispersion curves while on Love-dispersion curves its influence is negligible. Density, on the other hand, has no effect on the dispersion curves. Observations by Wathelet (2005) (in equation 3.6) suggested the relationship between $V_s$ and $V_P$ to be given by:

$$\upsilon = \frac{2V_S{}^2 - 2V_P{}^2}{2(V_S{}^2 - V_P{}^2)} \qquad 3.6$$

This relationship is the Poisson's Ratio, denoted by (υ). Reynolds (1997) observed that the values of this ratio ranged from 0 to 0.5 for all geologic materials, with the highest being 0.49 in clay and the lowest being 0.05 in hard rocks.

A misfit is the difference between the calculated dispersion curve and the experimental dispersion curve. If the data curve is affected by an uncertainty estimate, misfit, according to Wathelet (2005) in equation 3.7, is given by:

$$\text{misfit} = \sum_{i=1}^{n_F} \frac{(x_{di} - x_{ci})^2}{\sigma_i^2 n_F} \qquad 3.7$$

where $x_{di}$ is the velocity of data curve at frequency $f_i$, $x_{ci}$ is the velocity of calculated curve at frequency $f_i$, σi is the uncertainty of the frequency samples considered, $n_F$ is the number of frequency samples considered. If no uncertainty is provided, σi is replaced by $x_{di}$ in equation (3.7) (Wathelet, 2005).

# CHAPTER 4: MATERIALS AND FIELDWORK METHODS

## 4.1 Introduction

For this research, 3-component high sensitivity broad band sensors were laid out in a near-circular array configuration to record natural Earth's vibrations in Ahero area; part of the larger Nyanza basin, Kisumu County. The fieldwork was part of a larger project supervised and co-ordinated by the Geophysical Technology & Operations (GT&O) Group, Tullow Oil Ltd.

## 4.2 Desktop Studies

Literature covering the horizontal to vertical spectral ratio and frequency wave number techniques was studied. An overview of literature covering the structure and geology of study area and the entire region was also carried out. Additional publications on the methods of deployment and recovery, processing and analysis of passive seismic data were also studied. These included published scientific articles, published reports, maps and also operational manuals.

## 4.3 Methodological Approach

The main methodological approach involved deployment of Guralp Systems sensors in the field in standalone stations and also in an array configuration designed to yield specified minimum and maximum array resolutions. The steps involved in array noise processing were summarized in figure 4.1.

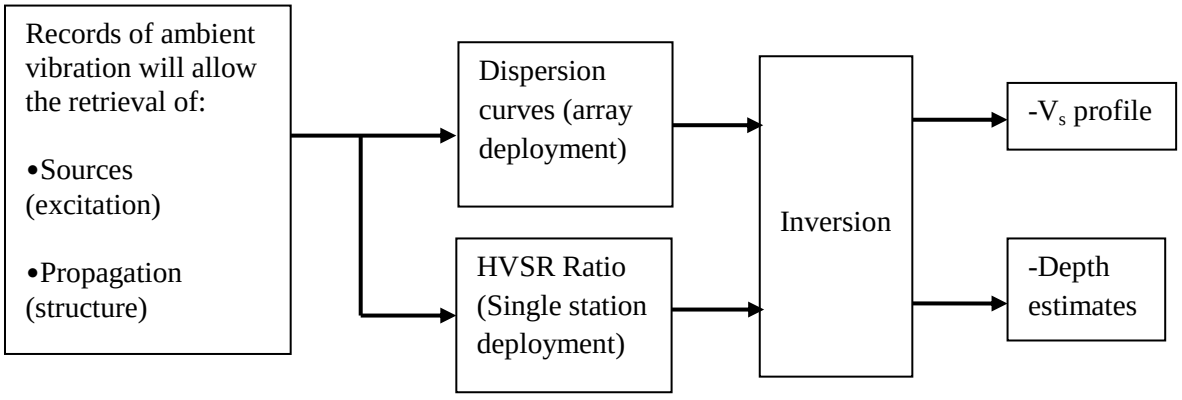


*Figure 4.1: A summary flow chart of the steps employed in carrying out the research. Adopted from www.geopsy.org (2005)*

### 4.3.1 Materials

Various materials were essential in carrying out this research, both in the fieldwork and also in the laboratory. The most crucial materials that aided the recording, retrieval and analysis of data for the research are briefly discussed in the following subsections.

#### 4.3.1.1 Guralp CMG-6TD Seismometers

These are low frequency (0.03 Hz) three (3) component waterproof broadband sensors designed for installation in a wide range of environments. The working temperature range for the sensor is assigned as -20°C to +80°C. The sensors are powered using standard car batteries of 12V, 25Ah as its power range is rated between 10V and 28V direct current (DC), (www.guralp.com, 2014).

The sensors have an in-built on-board 24-bit digitizer with configurable outputs hence facilitating desired calibration and its masses do not require locking/clamping during transport. The sensors record vibrations from all directions using the same concept as a conventional modern seismometer. Data downloading from this instrument was done over fire wire cable connected to an external specially-dedicated hard drive and then to a computer. Data output was in a special format supported by both the sensor and the specially made hard drive called Guralp Compressed Format (GCF) (www.guralp.com, 2014).

#### 4.3.1.2 GPS Receivers/Antennae

The antennae are designed to operate completely automatically once connected to power supply without configuration or initialization. A three dimensional (3D) fix (a measure of the time required for a GPS receiver to acquire satellite data-carrying signals and triangulate/calculate its position which includes latitude, longitude and altitude/elevation) was usually obtained within a short time after connection to power supply. The antennae were connected to the sensors where they were directly linked to the digitizers in the seismometers hence providing an extremely stable clock source to avoid data jitter and ensured a time-stamp for the data by synchronizing the instrument position and clock with the available satellites. From this synchronization, the status information, i.e., the number of satellites available, time of synchronization the position (latitude and longitude coordinates) and elevation of the instrument deployment location were also obtained.

The receivers are made of waterproof plastic casings allowing them to be adaptable to a wide range of temperatures. The accuracy of positioning for these receivers was within centimetres depending on the satellite visibility. Their low power consumption rates of <150mW is thus ideal for use with a car battery.

#### 4.3.1.3 Scream Software

"Scream" is an acronym for Seismometer Configuration Real-time Acquisition and Monitoring. This is a freely available software application (on request to Guralp Systems Ltd, at www.guralp.com) which was installed in two average computers running on Microsoft Windows 7. This application facilitated the configuration and monitoring of the instruments during deployment, recording and downloading of data. It also made it possible to carry out data integrity checks as well as mass positioning and GPS statuses. The software had many interfaces including networking features, and also different interfaces for Real-time conversion of data into different formats. In this project, however, only the Guralp Compressed Format (GCF) for data transfer was used.

#### 4.3.1.4 Other Items And Tools

Four portable hard drives specially designed to withstand hostile field environments by being encased with a durable rubber, shock resistant sleeve were used for storage and transport of data. Their storage capacity was usually 100 gigabytes (GB).

Field sheets were necessary for making notes of any anomalies noticed with sensors and also the general ground conditions that maybe useful for reference during processing. Cables, connectors, laptops installed with 'Scream' software and a tool bag containing all necessary accessories for aiding deployment was also provided.

### 4.3.2 Field Methods

#### 4.3.2.1 Deployment

Different deployment techniques are available for deployment of Guralp equipment depending on the environment in which acquisition is taking place and the purpose. In this project, the most convenient method was chosen for best results.

The Deployment of the L4 array was in a near circular configuration and designed to have a maximum penetration depth of up to 3km dictated by the diameter of the array, and a

minimum penetration depth of 250m dictated by the shortest distance between two stations (interdistance) as shown in figure 4.2. Field work preparation such as instrumental checks and public sensitization were carried ahead of the survey. Hand-held GPSes were used for navigation to desired locations following pre-plotted survey design. A quick survey of the location was done to establish if the point was in a desired location or needed to be relocated. For example, points that were traced to under trees were moved to a more open ground to allow visibility to satellites by the GPS antennae connected to the instrument.


*Figure 4.2: Satellite image of showing the near-circular L4 array and stand alone stations (in yellow dots), courtesy of GTO Team, Tullow Oil Ltd*

Remarks would then be made in the deployment field sheet as to why the point was offset. After being satisfied with the location, a hole of up to 60 centimetres deep was dug as close to the point as possible using a pick and a shovel for burying the sensor. The holes would be conveniently circular to take shape of, but slightly wider than, the sensor. The base of the hole was always made as level as possible to enable the sensor to rest upright and have all masses naturally centred. This also ensured maximum coupling of the base of the instrument with the ground. The power source and all cables were also buried in a second hole about 30cm from the sensor for security reasons. The sensors and power source were then placed in separate water proof jackets and lowered carefully into their respective holes as shown in figure 4.3. Using a compass, the sensor was aligned to true north guided by an arrow marked

'north' on it and connections to the instrument and GPS antenna (figures 4.3.and 4.4). The antenna was also securely pinned to the ground as close as possible to the instrument as it also helped in locating where the instrument was buried during recovery.

*Figure 4.3: Field deployment of equipment*

From the 'Scream' software, the waveform was checked to make sure the sensor was working well before completely covering it.

All the instruments in the arrays were left to simultaneously record for at least 48 hours before recovering them. Several stand alone stations were also deployed in strategic locations outside the array to provide additional information on the HVSR and depth estimates using the same procedure.

A general connection is illustrated in figure 4.4. The cable disappearing to the left hand side of the photograph is the power cable that connects to a battery.

*Figure 4.4: Various connections to the instrument ready for deployment*

#### 4.3.2.2 Recovery

This entailed demobilizing stations and transporting everything to the office for data downloading or retrieval. This was done with a lot of care to avoid damaging the instrument, cables and the battery. A general inspection of the surrounding for any abnormalities that might have happened was always done before beginning the recovery and notes taken. For example, interference by wild animals during the night might cause breakages to cables, they might knock down the GPS antenna thus causing loss of satellites and subsequently interfering with the data. Restoration of the ground was then done by covering all holes with soil and any wastes collected and packed for disposal back in the camp.

### 4.3.3 Laboratory Methods

In the laboratory, three main data processing and analysis techniques were applied. These included: the horizontal to vertical spectral ratio (HVSR), frequency wavenumber (F-K) and inversion of the output curves for velocity profile retrieval. These are discussed separately in the following subheadings.

#### 4.3.3.1 HVSR

The horizontal to vertical spectral ratio is a tool commonly used in geotechnical studies to investigate site effects as this ration yields a peak that coincides with the resonance frequency of the given site (Nogoshi and Igarashi, 1970; Nakamura, 1989; and Bard, 1998).

The compressed horizontal and vertical component signals for the appropriately selected recording time frame were loaded into GEOPSY software (geopsy.org, 2005). The signals were then plotted graphically using a graphic waveform tool available in the software to check their continuity. A minimum of six hours of common windows of continuous recorded signals was selected, cut and filtered appropriately. A Butterworth filter (band pass) was used for a frequency range of 0.10 Hz and 30 Hz to remove any instrument response. The continuous signals were then loaded into the HVSR processing tool in the software. The processing and output parameters were then set and the HVSR processing ran. The output was an HVSR curve for each stand alone station and an average HVSR curve for L4 array respectively.

#### 4.3.3.2 Frequency Wavenumber (F-K)

The process for preparing the signals ready for loading to the F-K processing tool in GEOPSY, an open source application software for analyzing the ambient wavefield downloaded from http://www.geopsy.org, was similar to the one used for the HVSR. The continuous signals were loaded into the F-K processing toolbox and an overall data time window with equal window length selected. The frequency sampling range was specified by selecting minimum and maximum frequencies as well as the output parameters. A dispersion curve was obtained as the end product.

#### 4.3.3.3 Inversion

The inversion process was done in GEOPSY software (geopsy.org, 2005) in two categories:

i) joint inversion of both the HVSR curve and the dispersion curve from the L4 array,

ii) inversion of the HVSR curve for single stand alone stations.

In both cases, the parameters for $V_P$, $V_s$, thickness, Poisson's ratio and density were chosen. The curves were set as the targets and re-adjusted/clipped to yield only peaks of low frequencies which are not likely to be influenced by local sources or human activity. The inversion process was then run to give the calculated curve. This curve was then compared with the observed curve (misfit) to see if the inversion gave a good result. If the curves didn't match, the inversion parameters were changed and inversion ran again. This iteration process was repeated until the observed and calculated curves matched.

The tuning parameters used for each of the categories in this inversion method were:

i) **$It_{max}$**- this is the number of iterations performed. This was set at two hundred (200) iterations for the stand alone stations outside the array and at a hundred (100) iterations for the L4 array stations as shown in figure 4.5.

ii) **$n_s0$**- the number of models chosen at random inside the parameter space at the beginning of the inversion. A hundred (100) models were chosen for both the stand alone stations and the L4 array stations (figure 4.5).

iii) **$n_s$**- the number of models to generate at each iteration. This was set at a hundred (100) models (figure 4.5).

iv) **$n_r$**- the number of best cells (cells with the lowest misfit) where the $n_s$ models are generated. Fifty (50) best cells were chosen for each iteration.

The **$It_{max}$**, **$n_s0$**, **$n_s$**, and **$n_r$** were set appropriately to control the inversion. More iterations were performed for the stand alone stations than the array because they have only a single input parameter (HVSR curve) as opposed to the array which has both the dispersion and HVSR curves as input parameters. A reasonably high number of iterations and models were selected to increase the chances of finding the best (lowest) misfit in the inversion. The inversion was then run to yield ground profiles. From the shape and resolution of these profiles, the $V_P$ and $V_s$ were adjusted accordingly and the inversion started again, with the density and Poisson's Ratio remaining constant until a reliable model was achieved.

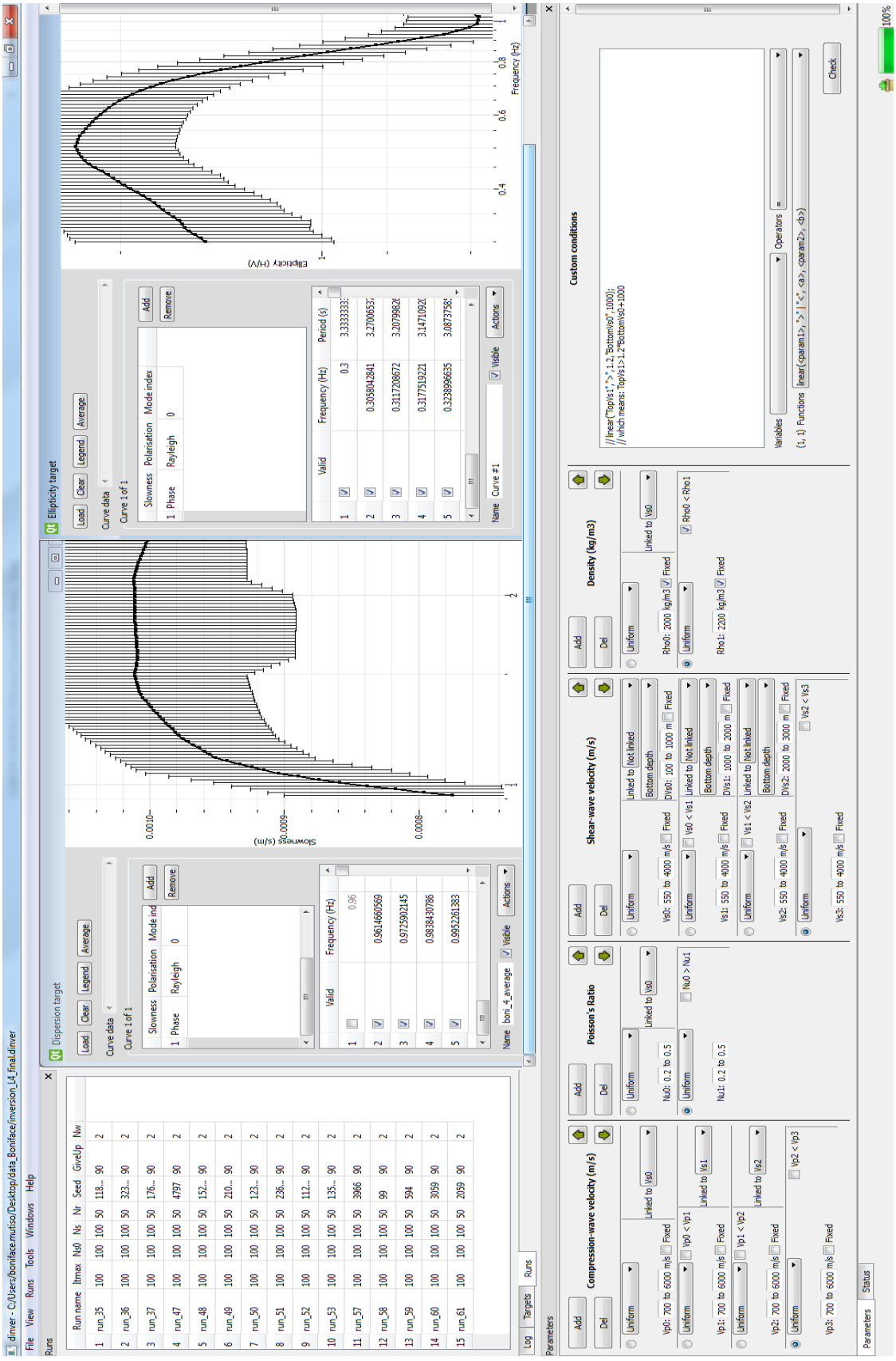

*Figure 4.5: Screenshot of various tools for dinver inversion tool in GEOPSY. The window to the top left shows Itmax, nso, ns, & nr and the number of runs. The middle section window enables importation and setting of the dispersion curve as a target while the one to the right facilitates setting of the HVSR as a target. The model parameters are set in the bottom window (www.geopsy.com, 2005).*

# CHAPTER 5: DATA ANALYSIS AND INTERPRETATION

## 5.1 HVSR

The HVSR was calculated for all stand alone stations comprising the L4 array. HVSR was also calculated for other selected stand alone stations that were not part of the L4 array. Four curves were chosen as samples to represent the rest of the stations of the L4 array: a set of curves with small second HVSR peak amplitudes (figure 5.1 and 5.2) from stations L4_11 and L04_07 respectively, and another set of curves with large second HVSR peak amplitudes (figure 5.3 and 5.4) from stations L04_18 and L04_13 respectively. The rest of the HVSR curves of the L4 array, are provided in the appendices.

### 5.1.1 HVSR For Array Stations

Results of the horizontal to vertical spectral ratio are presented in figures 5.1 and 5.2. The black solid curve represents the averaged HVSR of multi-coloured individual curves (resulting from different velocity classes of each iteration window) while the dotted black curves are the standard deviations of this averaged curve. The broad vertical grey line represents the averaged HVSR peak frequency and its standard deviation.

Figures 5.1 and 5.2 showed one main peak frequency at 0.45 Hz. All other stations in the L4 array showed a similar frequency irrespective of their location. This was inferred to be the resonance frequency of the study area.

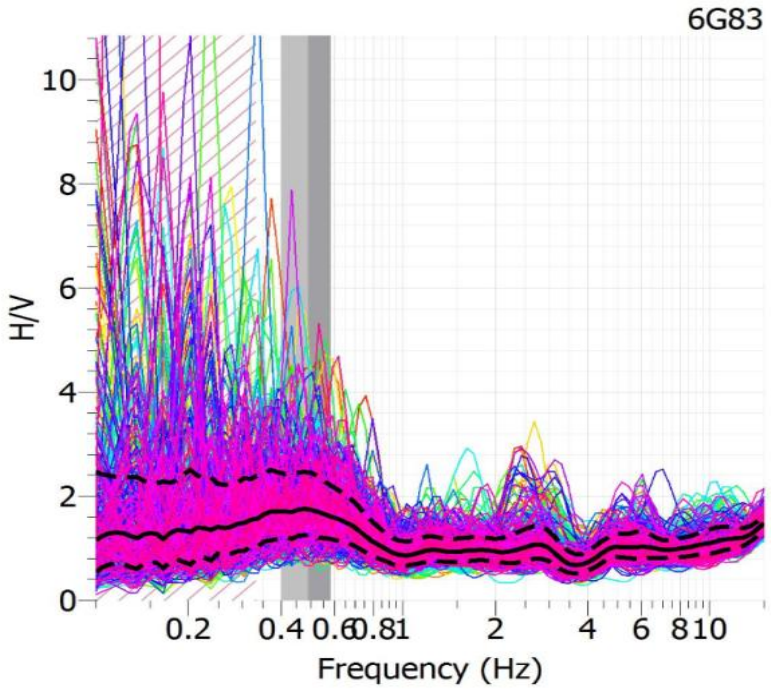


*Figure 5.1: HVSR curve of station L04_11 of the L4 array. The fundamental resonance frequency for this station was 0.45Hz and a second HVSR peak was inferred at 3Hz.*

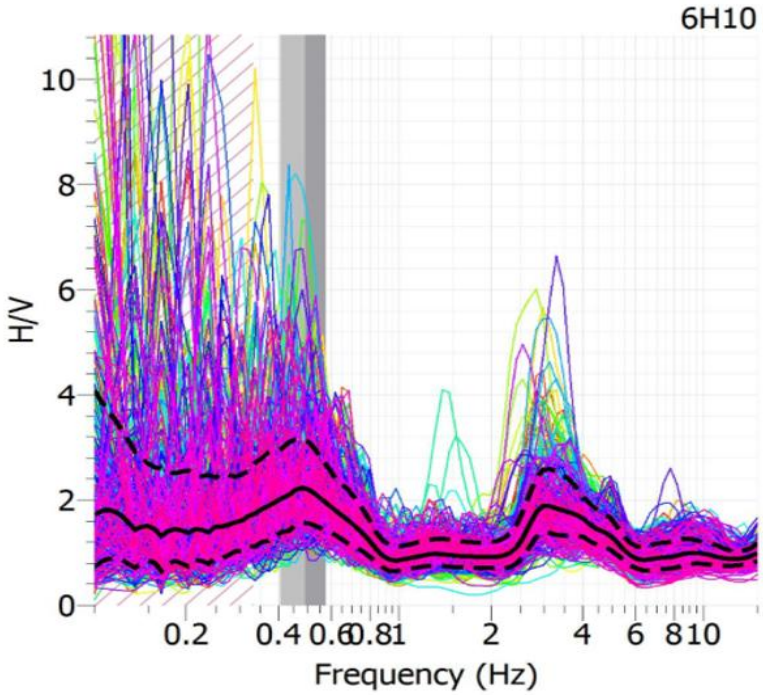


*Figure 5.2: HVSR curve of station L04_07 of the L4 array. The fundamental resonance frequency is at 0.45Hz and a second clear HVSR peak at 3Hz*

The presence of a second peak at about 3 Hz (figures 5.1 and 5.2) could indicate the presence of higher modes of the surface waves. These are probably caused by localised sources, most notably human activities due to the fact that the array was located close to a road network and also at close proximity to Ahero town. Introduction of high frequency vibrations into the medium by moving trucks combined with the non-dispersive properties of the body waves were assumed to be the main reasons for retrieval of the second peak, following findings of different authors. Most notably, Bonnefoy-Claudet et al. (2006) performed simulations for a simple realistic site (one sedimentary layer over bedrock) characterized by a high impedance contrast and low quality factor, postulated that:

i. 'For ambient noise due to far sources within a layer, HVSR ratios exhibit two peaks, one is located at the resonance frequency and is produced by a mixture of fundamental Rayleigh waves and the non-dispersive waves. The other one that occurs at the first harmonic frequency of the resonance is due to non-dispersive waves, this could be produced by S-wave velocities along the sediment-to-bedrock interface';
ii. 'For ambient noise due to sources located within the bedrock, HVSR ratios exhibit two peaks at the fundamental and the first harmonic resonance frequencies; the vertical noise wavefield is strongly dominated by S-waves. HVSR ratios peaks are related to multiple S-waves resonance.'

Their conclusions, however, were only based on a single sedimentary layer overlying a bedrock and, therefore, need to be tested more over several sedimentary layers overlying a bedrock. In this study, however, only the fundamental mode is analysed. Although the proximity of human activities to the deployed stations seems to suggest the source of the higher frequency peaks to be of a local nature, more investigations, outside the scope of this work, are needed to evaluate the sources of the secondary peaks.

In the case of the second set of samples in figures 5.3 and 5.4, the second peak was found to be more than twice as big as the fundamental frequency and occurring at different frequencies. These peaks occurred at 6Hz and 5Hz, respectively, and local sources, e.g., cars, Ahero Town, the irrigation schemes in the area, etc, were the possible causes of the strong second HVSR peaks.

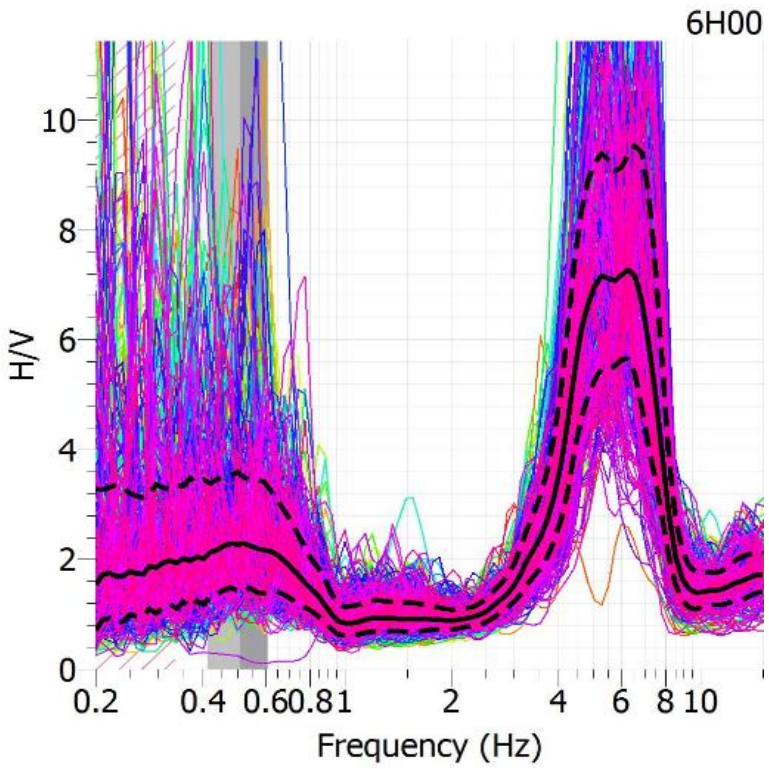


*Figure 5.3: HVSR curve of station L04_18 of the L4 array. The fundamental resonance frequency is at 0.45Hz and a second large HVSR peak at 6Hz*

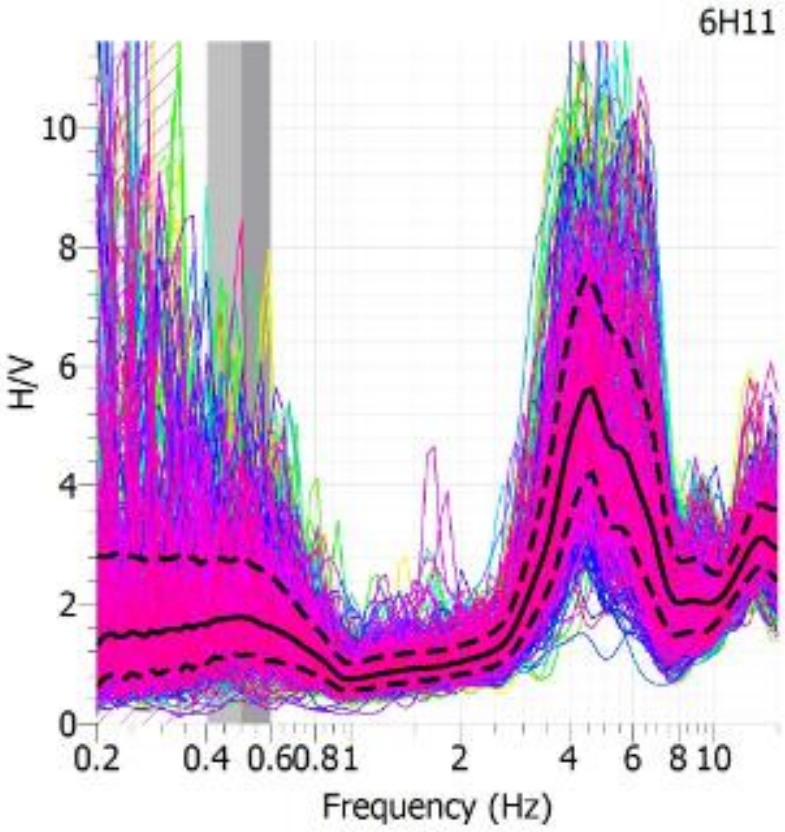


*Figure 5.4: HVSR curve of station L04_13 of the L4 array. The fundamental resonance frequency is at 0.45Hz and a large HVSR peak at 5Hz*

A cumulative plot of the HVSR curves for each station of the L4 array was plotted as shown in figure 5.5. A general stability of the first peak supported the hypothesis that fundamental frequency across all the stations was not influenced by the local sources whereas the unstable second peak was possibly as a result of external interference by local sources.

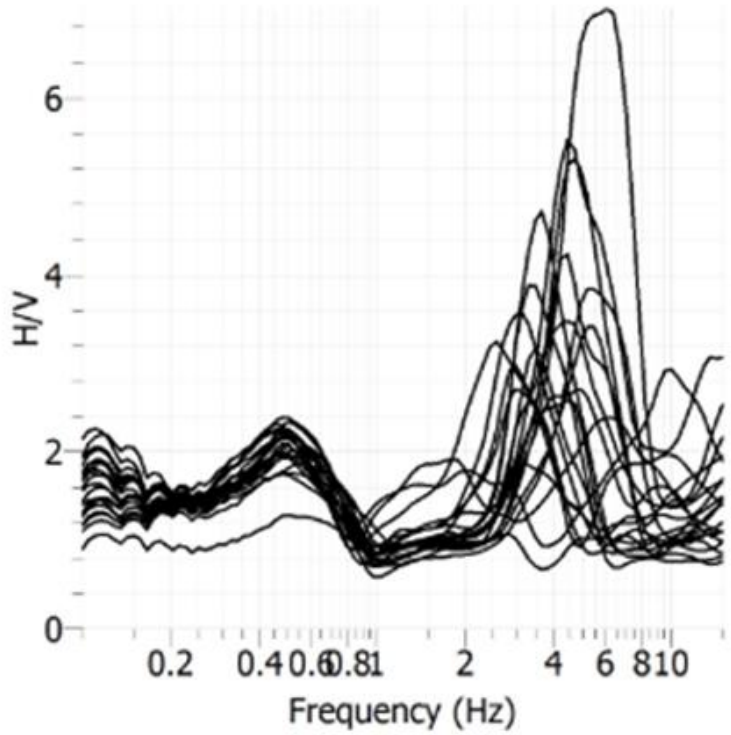


*Figure 5.5: A cumulative plot of all the HVSR curves from each individual L4 array stations.*

The HVSR output of the L4 array was then computed as shown in figure 5.6 by averaging the HVSR curves of the individual array stations.

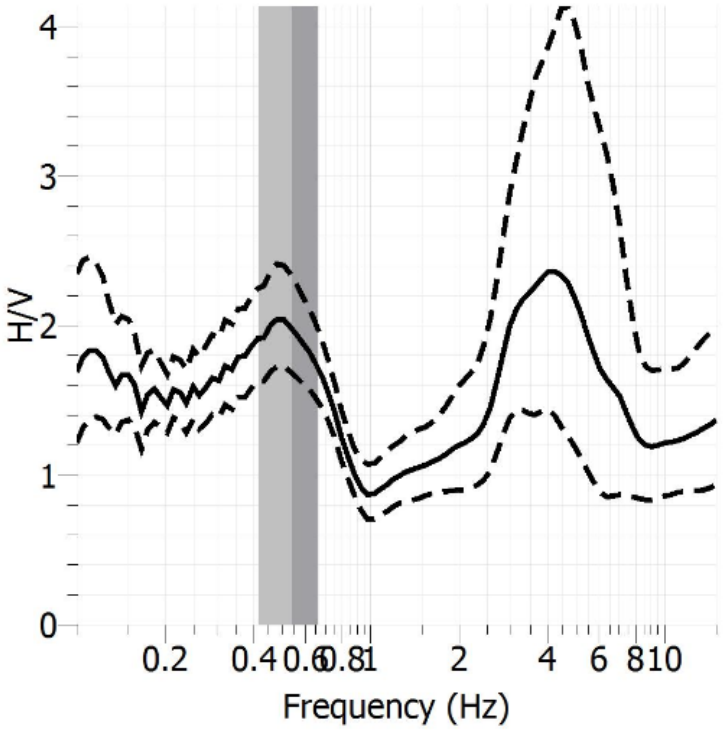


*Figure 5.6: HVSR output of the L4 array. This is the average of individual HVSR curves of the L4 array stations in figure 5.5*

### 5.1.2 HVSR For Stand Alone Stations

HVSR was performed for three stand alone stations that were not part of the L4 array to provide a constraint of the area fundamental resonance frequency. These included: station A_16, station A_19 and station A_25. The location of station A_25 on NT4-89 seismic line provided independent results during inversion that was compared to those of the L4 array and 2D seismic survey. The HVSR results of the three stand alone stations are presented in the following subsections.

#### 5.1.2.1 Station A_16

Station A_16 (sensor 6G92) yielded two HVSR peaks as seen in figure 5.7. The fundamental resonance frequency peak was inferred at approximately 0.45Hz (figure 5.7). This frequency was consistent with the frequencies obtained from the array stations and further indicated that local sources and local geology were not influential of this frequency. A secondary peak with large amplitude was obtained at a frequency of 4Hz suggesting probable influence of underlying geology or possibly due to localized vibrations caused by human activity.

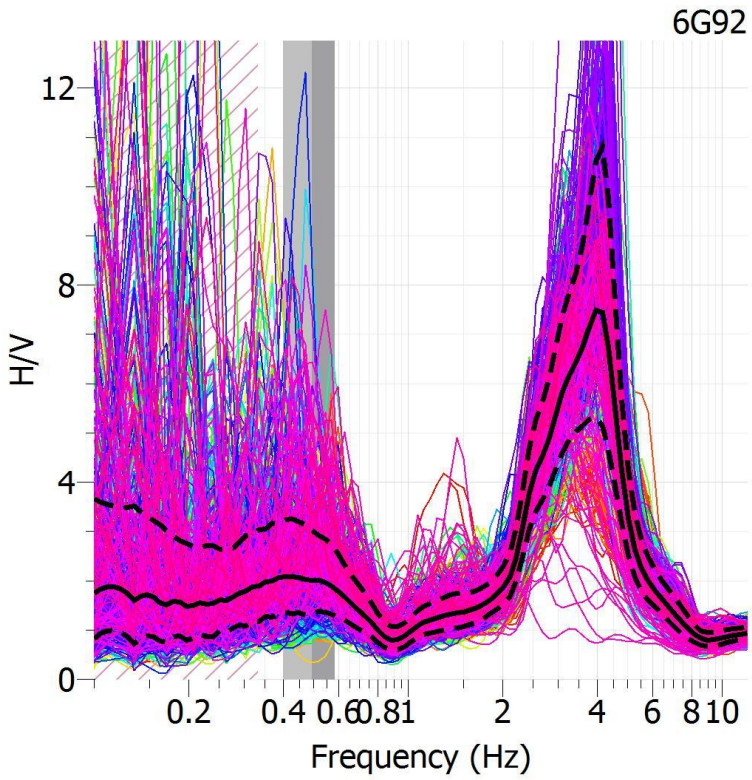


*Figure 5.7: HVSR curve showing fundamental frequency peak of station A_16 at 0.45Hz and a secondary HVSR peak at 4Hz*

#### 5.1.2.2 Station A_19

The fundamental HVSR peak for this station was inferred between 0.4 and 0.6Hz while three secondary peaks were obtained at frequencies 3Hz, 5Hz and 12Hz as shown in figure 5.8. The secondary peaks were probably due to influence of local sources.

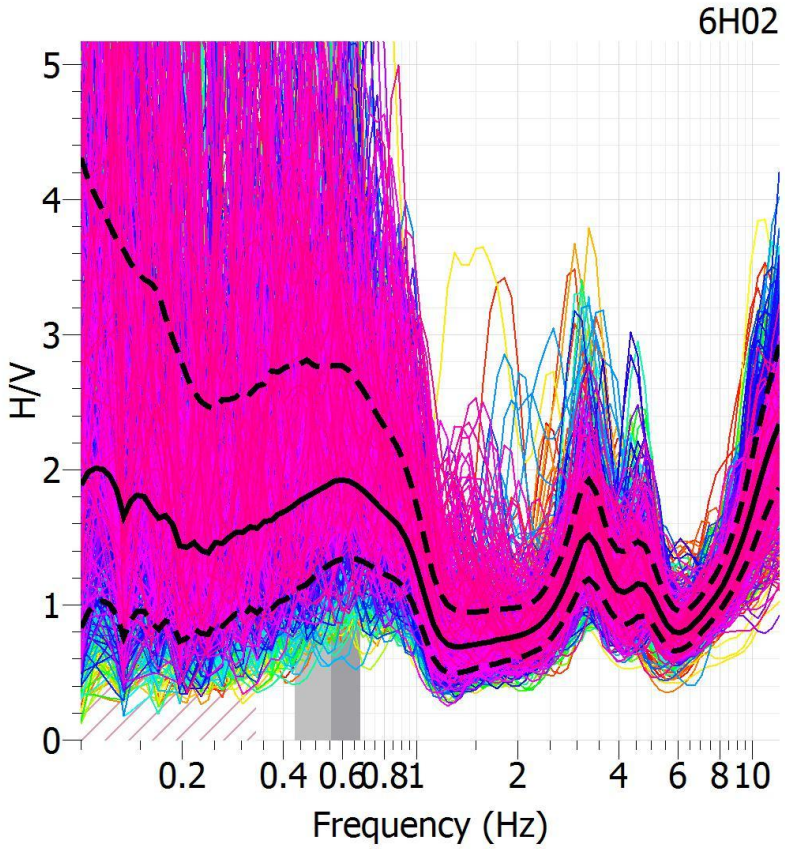


*Figure 5.8: Fundamental HVSR frequency peak at 0.45Hz and three more HVSR peaks of station A_19*

#### 5.1.2.3 Station A_25

Stand alone station A_25 yielded three peaks at 0.3Hz, 0.6Hz and 1.2Hz. The resonance peaks in this station seemed to be of a more complex shape with a less single defined main peak but rather a small range of frequencies as shown figure 5.9. However, this range of values of the resonance frequency was similar to those of the other stand alone stations.

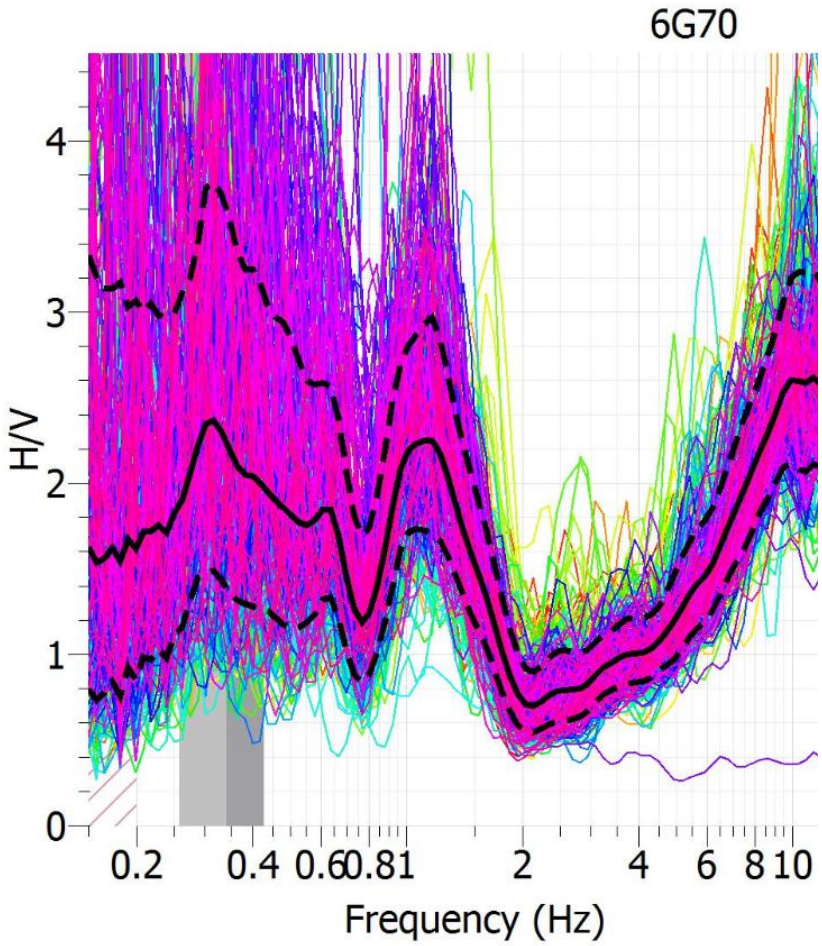


*Figure 5.9: Possible fundamental HVSR frequency peaks at 0.3Hz and 0.6Hz for station A_25*

### 5.2 Frequency Wavenumber (F-K)

The output of this technique on the L4 array was a colour chart of the dispersion curve (enclosed in black box) whose plot was slowness (inverse of velocity) versus frequency, as shown in figure 5.10. The dispersion curve together with its standard deviation was manually picked from this image and an average dispersion curve calculated from it in Max2curve statistical analysis tool in GEOPSY software as shown in figure 5.11 (geopsy.org, 2005).

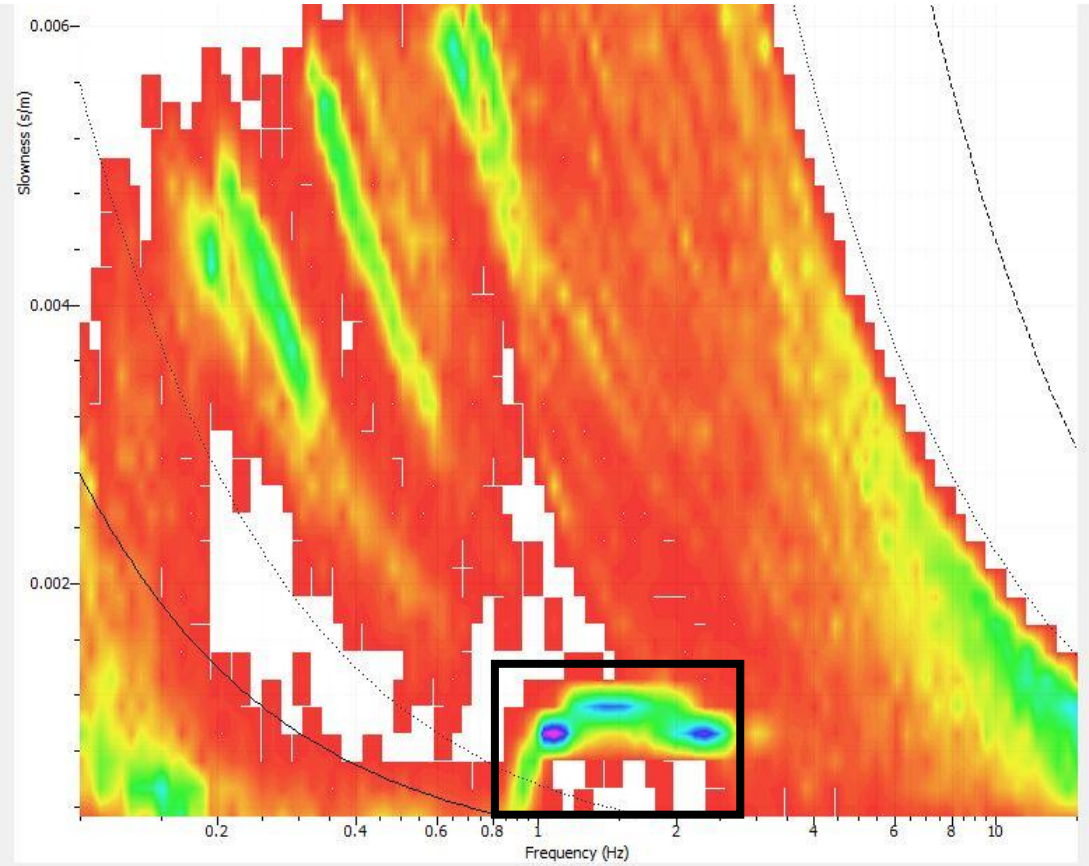


*Figure 5.10: Colour chart (image) of the dispersion curve calculated from L4 array.*

The bottom corners of the colour image in figure 5.10 is characterised by aliasing noise probably generated by lack of resolution coming from the array limits. The multicolours are as a result of different velocity classes while the white patches of this image are due to lack of data. The first bold curve on the left represents ½ $K_{min}$, followed by a second dotted curve representing the $K_{min,}$ then a third dotted curve representing ½ $K_{max}$ and finally to the extreme right is a bold dotted curve representing the $K_{max}$ as discussed in section 3.1.6.

An average of the slowness histograms performed in the Max2curve statistical analysis tool in GEOPSY software (geopsy.org, 2005) resulted in a line plot of slowness versus frequency including its error bars. The dispersion curve in figure 5.11 showed phase velocity (inverse of slowness) decreasing with increase in frequency. This curve was used as 'observed data' for the L4 array inverse problem discussed in section 3.1.7.

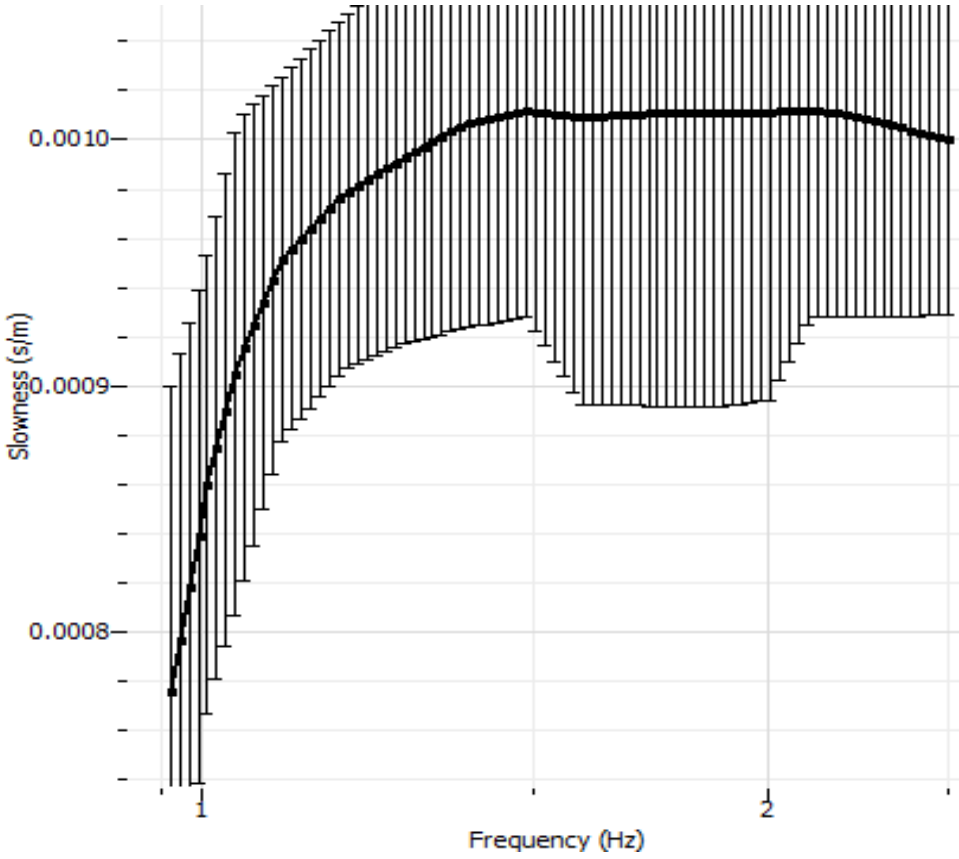


*Figure 5.11: The averaged dispersion curve from L4 array. The vertical lines are the error bars of this curve as calculated in GEOPSY.*

### 5.3 Inversion

The velocity averages obtained in this research, through inversion, are all estimates based on the passive seismic method and survey design; they are, therefore, used only for the purposes of this research. The non-uniqueness of the inverse problem yielded many velocity models that span in ranges, therefore, the results of this thesis should be treated as averages of these ranges. Velocities given in Table 3.1 (Bourbié, 1987) were used to compare with the velocity averages obtained from the inversion models. These velocities may, however, differ for the same rock type subjected to different conditions, e.g., fracturing, alteration, etc. They were, therefore, used with caution for general comparison purposes for this research and not as final velocities for the rock formations encountered in the area where this research was carried out. The goal of the inversion process was to obtain a quantitative velocity model evaluation among reliable model parameterizations, through iterations that fitted satisfactorily with the measured data. The final results in each location showed the variation of the velocity model with the misfit values of the best models (the ones with lowest misfit), and were shown in red colour in the output profiles which also serves as the lowest misfit for each model.

### 5.3.1 HVSR Inversion

The HVSR curves obtained from selected stand alone stations were inverted. Vp and Vs velocity models obtained for each location, results are shown in the following subsections.

#### 5.3.1.1 Station A_16

The inversion process yielded three (3) well resolved velocity contrasts (depth values indicated in the following profiles should be considered as average values of the depth interval of the best velocity models highlighted by the red section in the figures) for this station at approximately 170m, 550m and 1600m in depth as shown in figure 5.12 (a). At approximately 170m, the S-wave velocity increased from approximately 500m/s to around 1200m/s. A plot of the ellipticity curve, in figure 5.12 (b) to compare the error margin between the calculated and measured data yielded a low misfit of less than 0.1 in that the measured data (black curve) fitted well with the calculated data (red section).

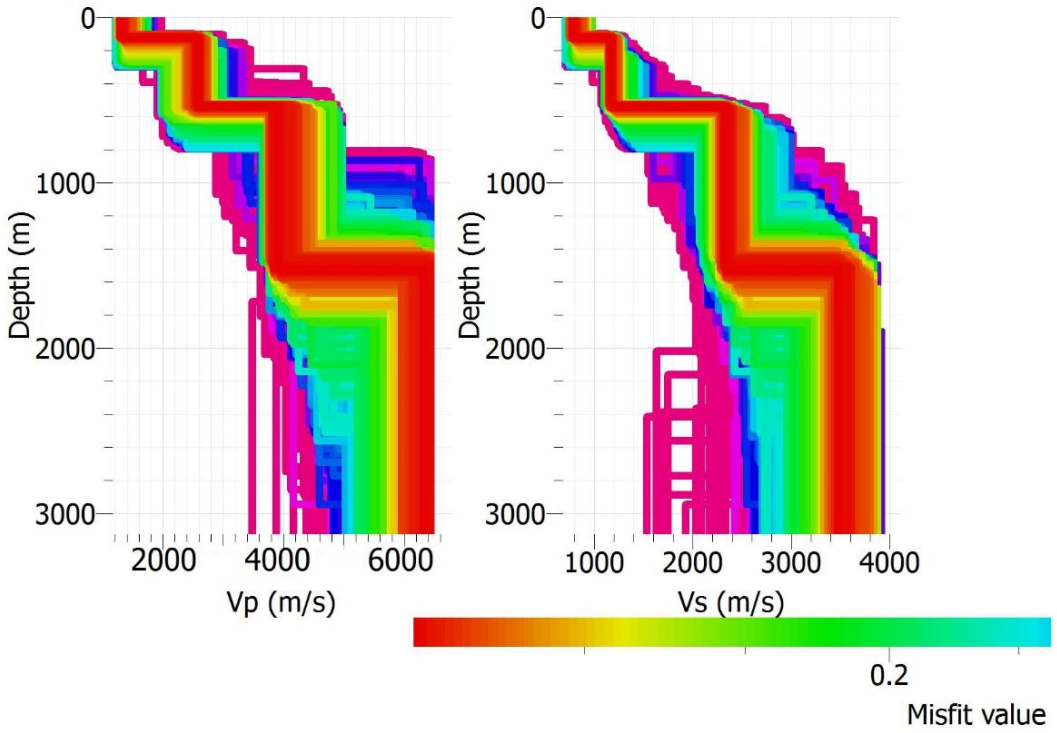


*Figure 5.12 (a): A normally dispersive $V_P$ and $V_S$ (m/s) velocity profile of station A_16 obtained through inversion of the HVSR curve of this station*

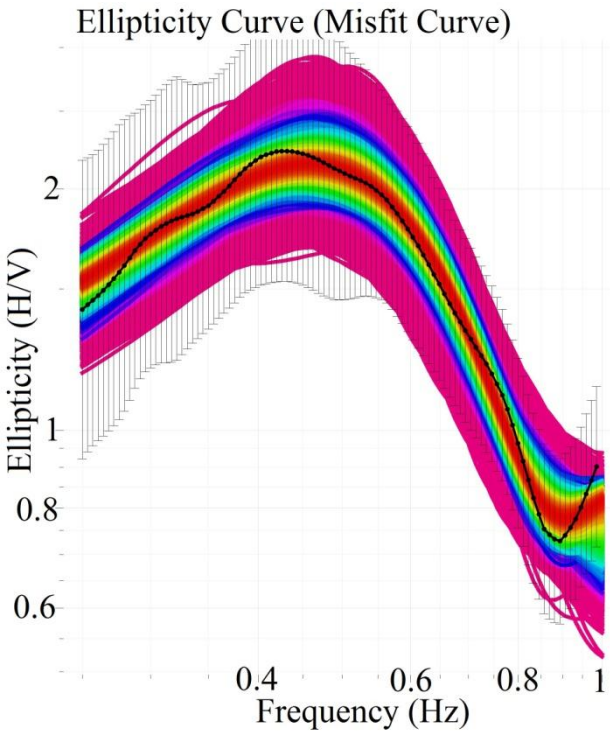


*Figure 5.12 (b): The corresponding ellepticity curve plot for station A_16 representing the misfit between predicted data and measured data.*

According to Bourbié (1987), see table 3.1, the velocity ranges associated with the first interface could be as a result of saturated clays. These water saturated clays were encountered during field work but lithological analysis is needed to confirm this result beneath the surface. A second interface occurred at a depth of approximately 550m/s and a third velocity contrast at an approximate depth of 1600m. These velocity interfaces are an indication of change in lithology. A normally dispersive profile predicts that velocities of different lithologies increase with increase in depth as a result of lithification and diagenesis.

#### 5.3.1.2 Station A_19

The output of the inversion process for station A_19 was also a velocity profile. Three velocity contrasts as shown in figure 5.13 (a) were obtained at depth estimates of 220m, 650m and 1500m. A low misfit was achieved between calculated and measured data as shown by figure 5.13 (b). The black curve representing measured data superimposed over the calculated data curve therefore suggesting a very narrow error margin of the data accuracy.

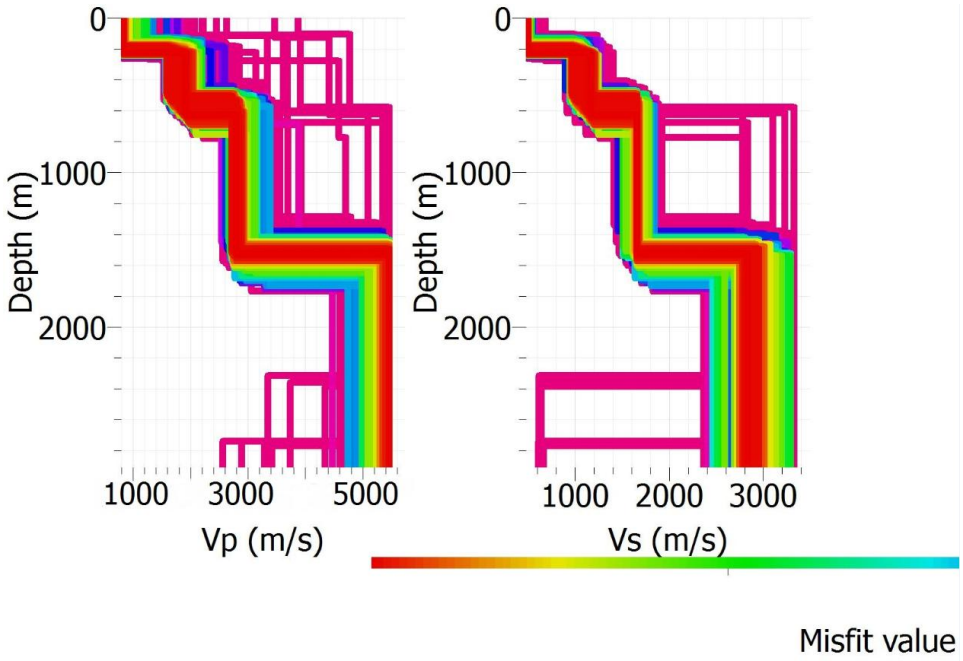


*Figure 5.13 (a): A VP and VS (m/s) velocity profile of station A_19 obtained through inversion of the HVSR curve of this station*

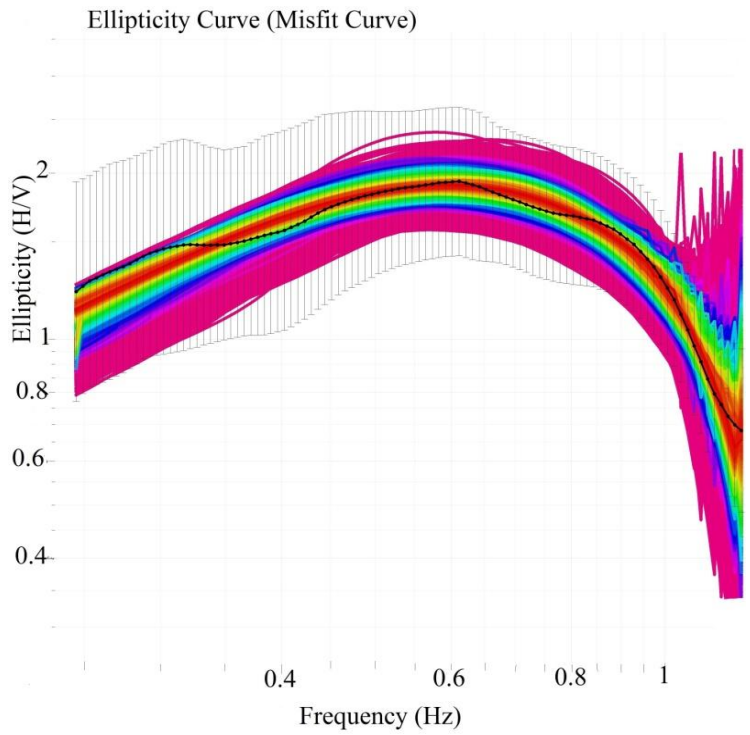


*Figure 5.13 (b): The model ellipticity curve for station A_19 corresponds to a low misfit between the predicted model (red curve) and the measured data curve (black curve).*

From table 3.1 (Bourbié, 1987) these velocity ranges seem to suggest Holocene sediments overlying Pleistocene sediments which also corresponds to Saggerson (1952) findings.

However, the results of the passive seismic analysis are strictly given as velocity ranges without any other supporting information to identify the actual nature of the rock lithology types thus more accurate analysis, e.g. lithological logs are needed to accurately infer the geology of the area.

#### 5.3.1.3 Station A_25

This station was located on the north-eastern end of seismic line NT4-89. Three velocity contrasts were obtained in the inversion model for this station at inferred depth estimates of 200m, 600m and 2600m as shown in figure 5.14 (a) whereas the ellipticity curve plot achieved a low misfit between the predicted model curve and measured data as shown in figure 5.14 (b). This station showed a deeper reflector at lower velocities than the other stand alone stations (including the L4 array in figure 5.15 (a)) as seen in figure 5.14 (a). There is a strong likelihood that the second interface is due to volcanics as further supported by the high reflectivity of this layer in the 2D vintage seismic stack in figure 5.18 (a).

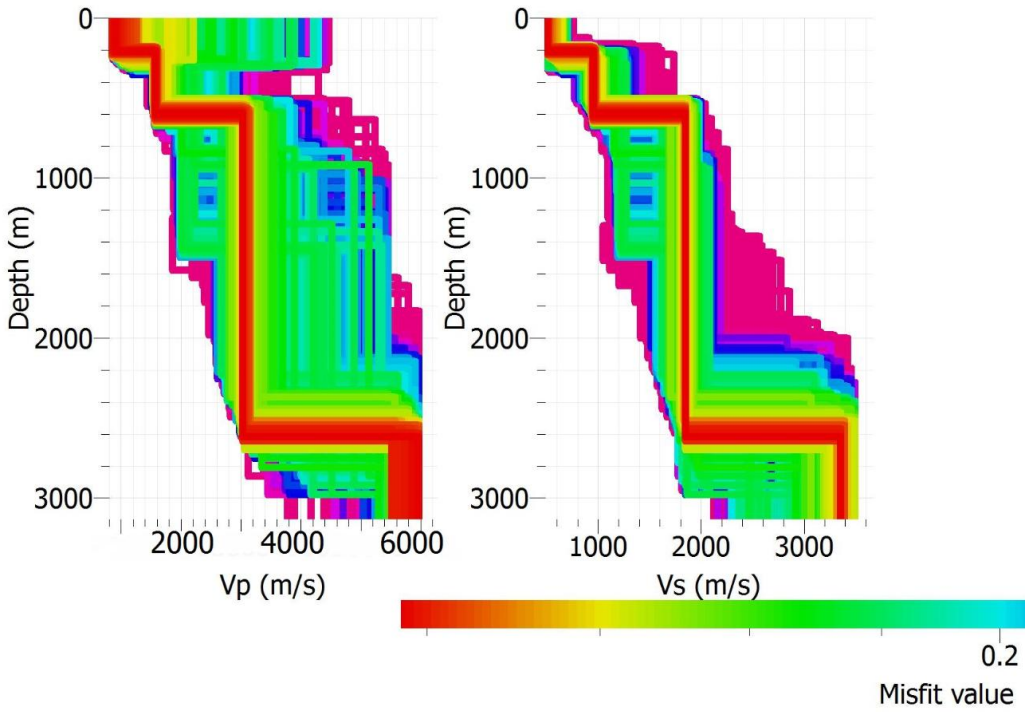


*Figure 5.14 (a): A normally dispersive $V_P$ and $V_S$ (m/s) velocity profile of station A_25*

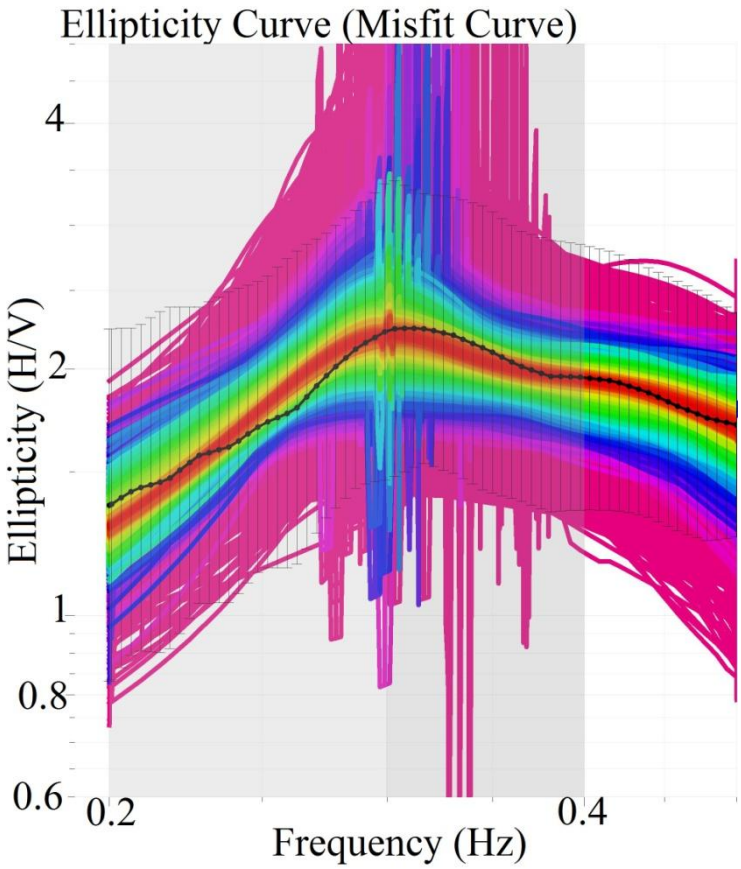


*Figure 5.14 (b): Low misfit between the predicted ground velocity model and measured data curve.*

The presence of volcanic rocks in the basin is evidenced by volcanic outcrops at the surface, as well as the surrounding escarpments which are also volcanic in nature. As the second interface is most likely due to volcanic rocks, characterised by high velocities, velocity inversions can be expected in a sedimentary basin with volcanic intercalation. High degrees of freedom in the inversion were thus allowed to explore this possibility. Velocity inversions were detected as some of the output models showed reversed velocities. Martin et al. (2015) obtained an inverse velocity profile in this area at similar average depths which is in agreement with the hypothesis that this region is characterized by volcanic-sediment velocity contrasts.

### 5.3.2 Joint Inversion

The array average HVSR (figure 5.6) was jointly inverted with the dispersion curve (figure 5.11) obtained from the L4 array. Two clear interfaces were encountered at approximate depths of 120m and 550m while a third velocity contrast, which was not well resolved, was encountered at an approximate depth of between 900m and 1400m as shown in figure 5.15 (a).

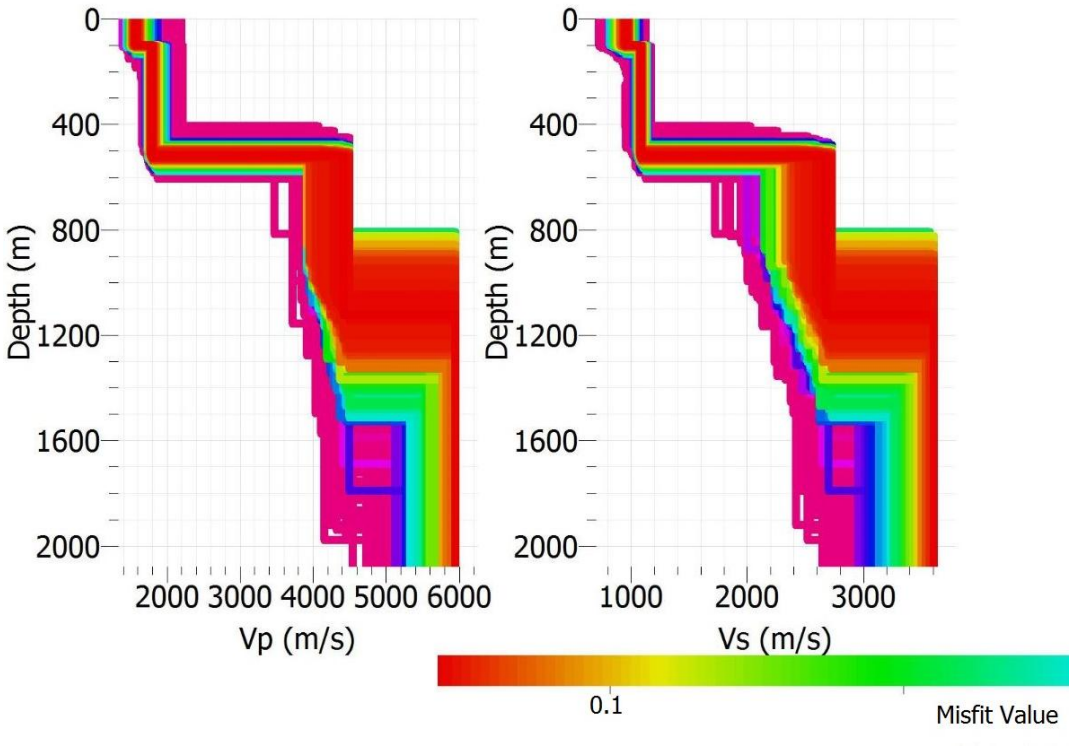


*Figure 5.15 (a): A normally dispersive VP and VS (m/s) velocity profile of the L4 array achieved by jointly inverting the L4 array dispersion curve and the averaged L4 array HVSR curve.*

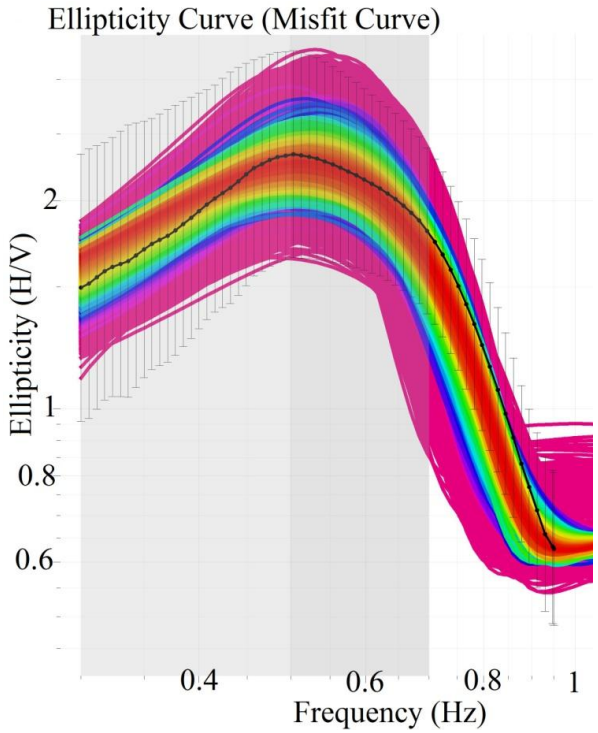


*Figure 5.15 (b): The corresponding ellipticity plot for the L4 array representing a low misfit between the predicted model and the measured data curves.*

A similar trend as that of the three stand alone stations analysed early was seen in the L4 array output. The first contrast was most likely due to lithological contact between a layer of loose sediments and another slightly more consolidated sedimentary unit. According to Saggerson (1952), the first layer could be linked to Holocene sediments dominated by water saturated clays. This seemed to be confirmed by observations made in the field during fieldwork. Literature on the geology of this area suggests that this unit could be underlain by lacustrine (mostly lake) sediments or a porous sandstone formation of the Pleistocene period. The second interface obtained in the inversion model could be associated with Miocene sediments (more likely to be limestones) or weathered tertiary volcanics following Saggerson (1952). The last interface was not well resolved as a result of poor signal to noise ratio and was thus given as a range between 900m and 1400m. These observations are, however, only based on surface geology literature and cannot be used with confidence to interpret and also compare with the results obtained from the passive technique. Well log data would offer more reliable and comprehensive results to counter-check with the passive results.

### 5.4 Two Dimensional (2D) Active Seismic Stacks

Three 2D seismic stacks from three seismic lines of a survey carried out in 1989 were provided by Tullow Oil Ltd. These seismic lines were: NT1_89, NT3_89 and NT4_89 running east to west, north-west to south-east and north-east to south-west, respectively. The L4 array was located at the intersection of two lines: NT1_89 and NT3_89, while stand alone station A_25 was located on line NT4_89. Time to depth conversion was carried out, referenced to 1200m ASL (after Martini et al., 2015) as shown in figures 5.16 (a), 5.17 (a) and 5.18 (a).

The seismic data from Line NT1_89 generally showed bright seismic reflectors at estimated depths of between 200m and 600m indicating a zone of a high velocity compact formation; probably a zone of volcanics. The L4 array was located between Common-Depth-Point (CDP) 687 and 794 as shown by the blue arrow in figure 5.16 (a). There is a high comparability of the depth of the first high velocity seismic horizon of the active seismic with that inferred from the L4 array in figure 5.16 (b) at a depth estimate of 180m. Below 600m, there was a lot of scattering as a result of loss of signal strength, (low signal to noise ratio) caused by presence of volcanics overlying sediments (Martini et al., 2015), and hence no seismic horizon matching the third velocity contrast highlighted by the passive seismic technique could be picked.

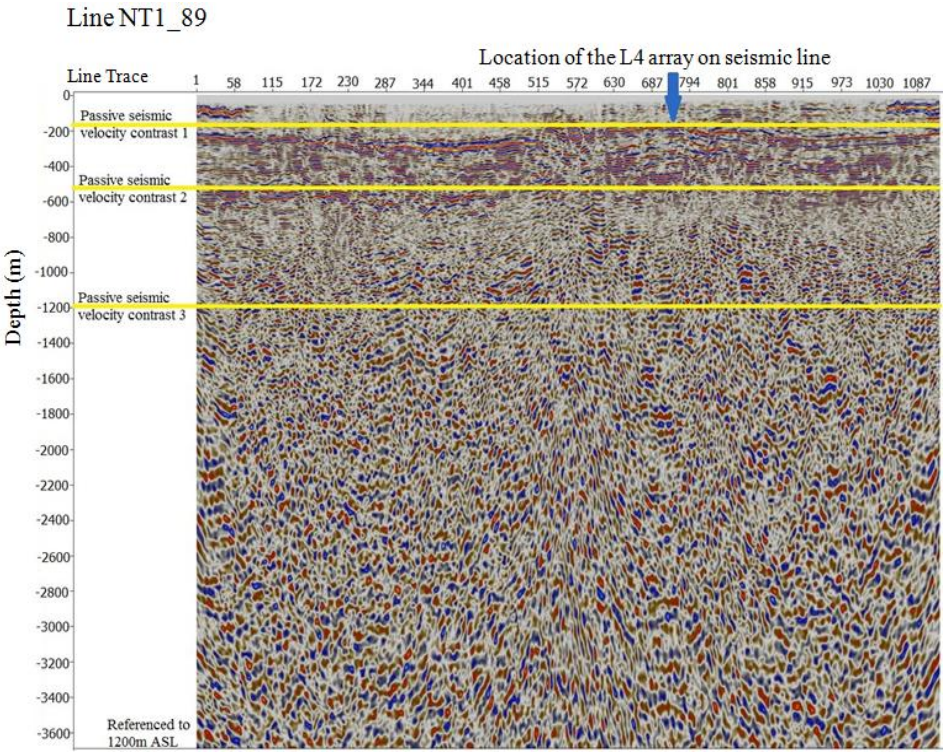


*Figure 5.16 (a): 2D vintage seismic stack from seismic line NT1_89 with both the location of the L4 array highlighted by the blue arrow and the three velocity contrast depth estimates of the passive seismic technique shown in yellow lines. Source: Tullow Oil Ltd*

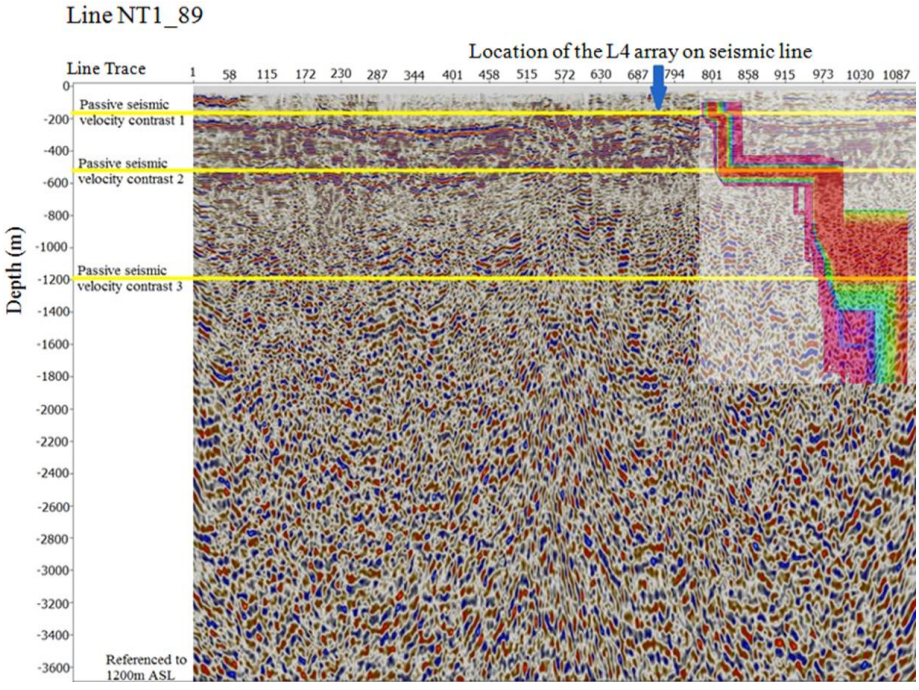


*Figure 5.16 (b): Comparison of 2D active seismic data with the results of the L4 array output of the passive seismic technique. Source: Tullow Oil Ltd*

The loss of signal strength below the second reflector of the active seismic strongly supports the hypothesis that this geological formation is highly likely to be volcanics and that below it there is a deeper sedimentary unit, and hence suggesting the basement in this basin is deeper than initially thought. This hypothesis is in agreement with the passive results obtained from the L4 array which presented a third layer at a depth approximated as 1200m.

On line NT3_89, the L4 array was located at CDP 58. The depths to basement estimates for this seismic line were also comparable to those of the L4 array and those of line NT1_89. This line, however, shows some coherency of energy for a third layer which as matches the one given by the passive technique as shown in figure 5.16 (a). The brightness of the second horizon from the active seismic suggests a high velocity layer underlain by a third lower velocity zone.

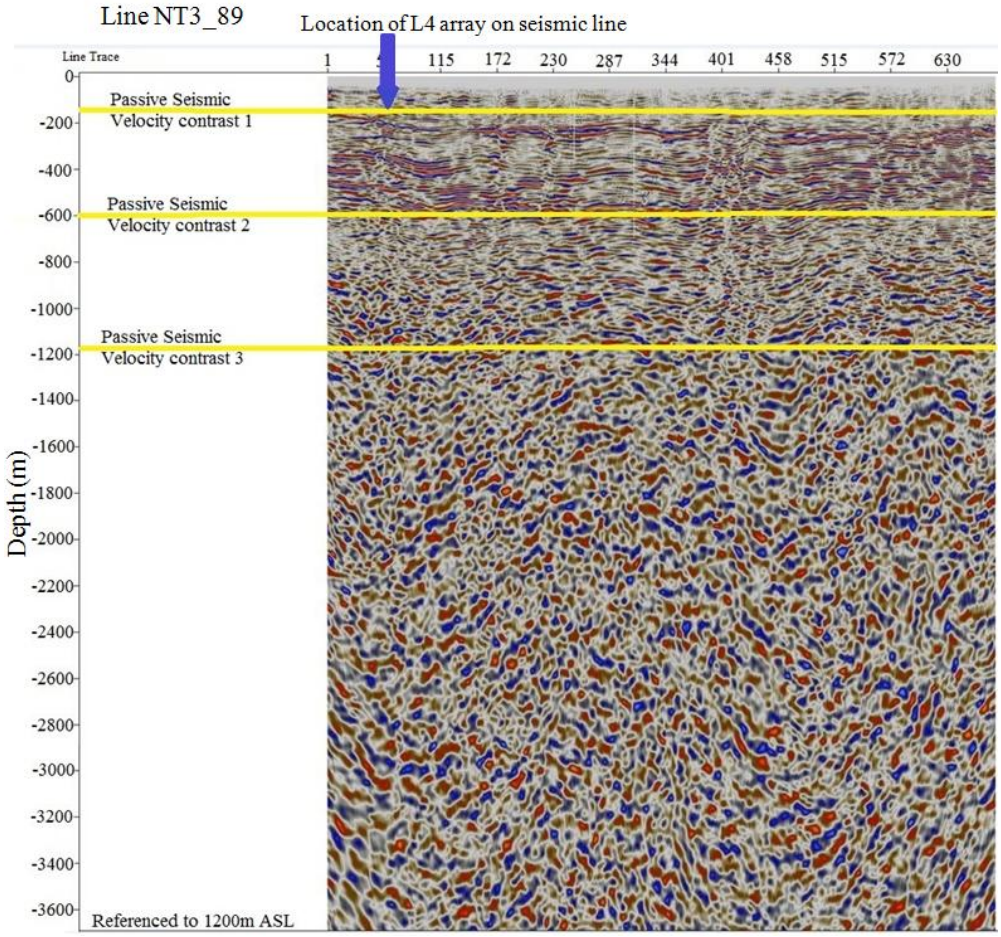


*Figure 5.17 (a): L4 array location on line NT3_89. Source: Tullow Oil Ltd*

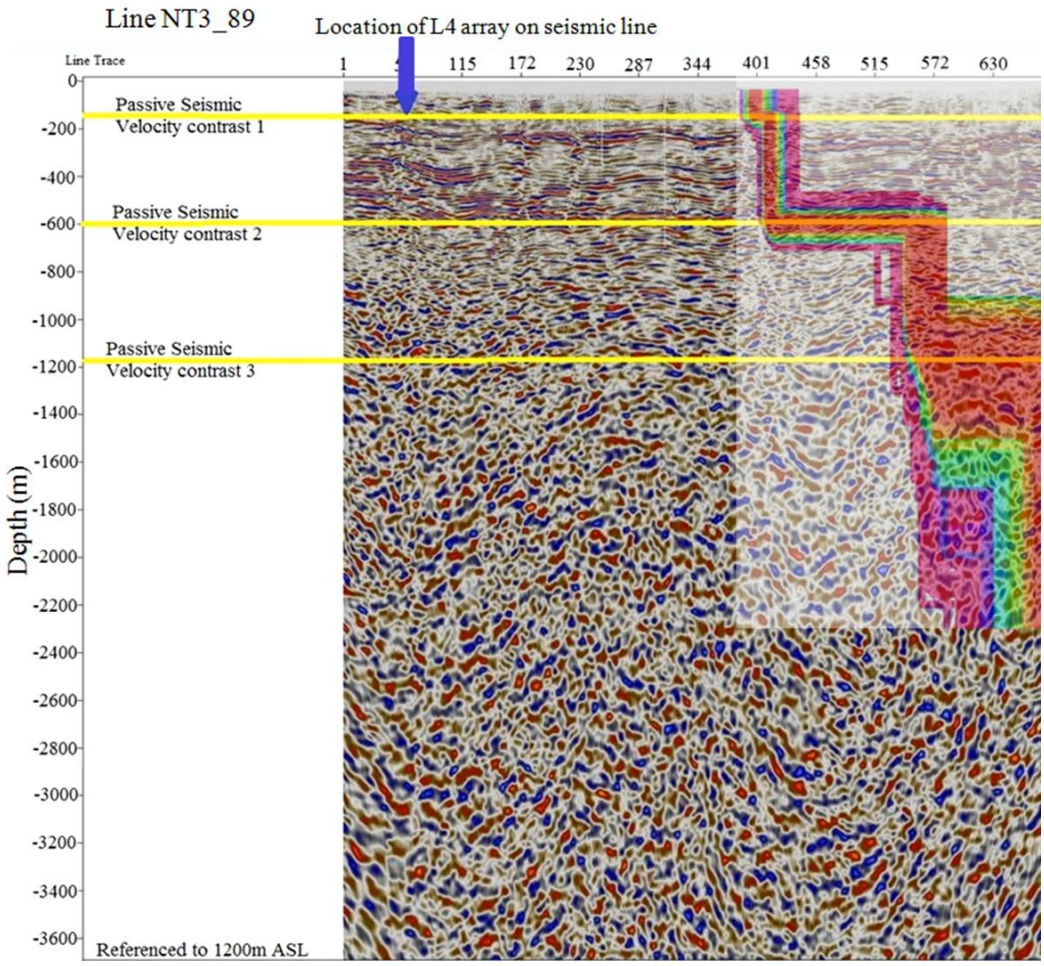


*Figure 5.17(b): L4 array velocity model superimposed on active seismic stack of seismic line NT3_89. Source: Tullow Oil Ltd*

Below 1200m of this stack, there was extreme attenuation and loss of coherency of energy hence no horizon could be picked below this depth. The passive seismic technique as well did not produce any horizons below this depth for the L4 array.

The stack from Line NT4_89, on which station A_25 was located, was slightly different from the other two presented earlier. Whereas the previous seismic lines showed horizontal layers, the layers in this line are dipping south westerly towards the lake and faulted as shown in figure 5.18 (a). At the location of the station A_25, there was good correlation between the active seismic and passive seismic at depth estimates of between 200m and 600m as shown in figure 5.18 (b). The second seismic horizon, however, seems to be splitting into several smaller horizons, which could be as a result of localized events, away from station A_25.

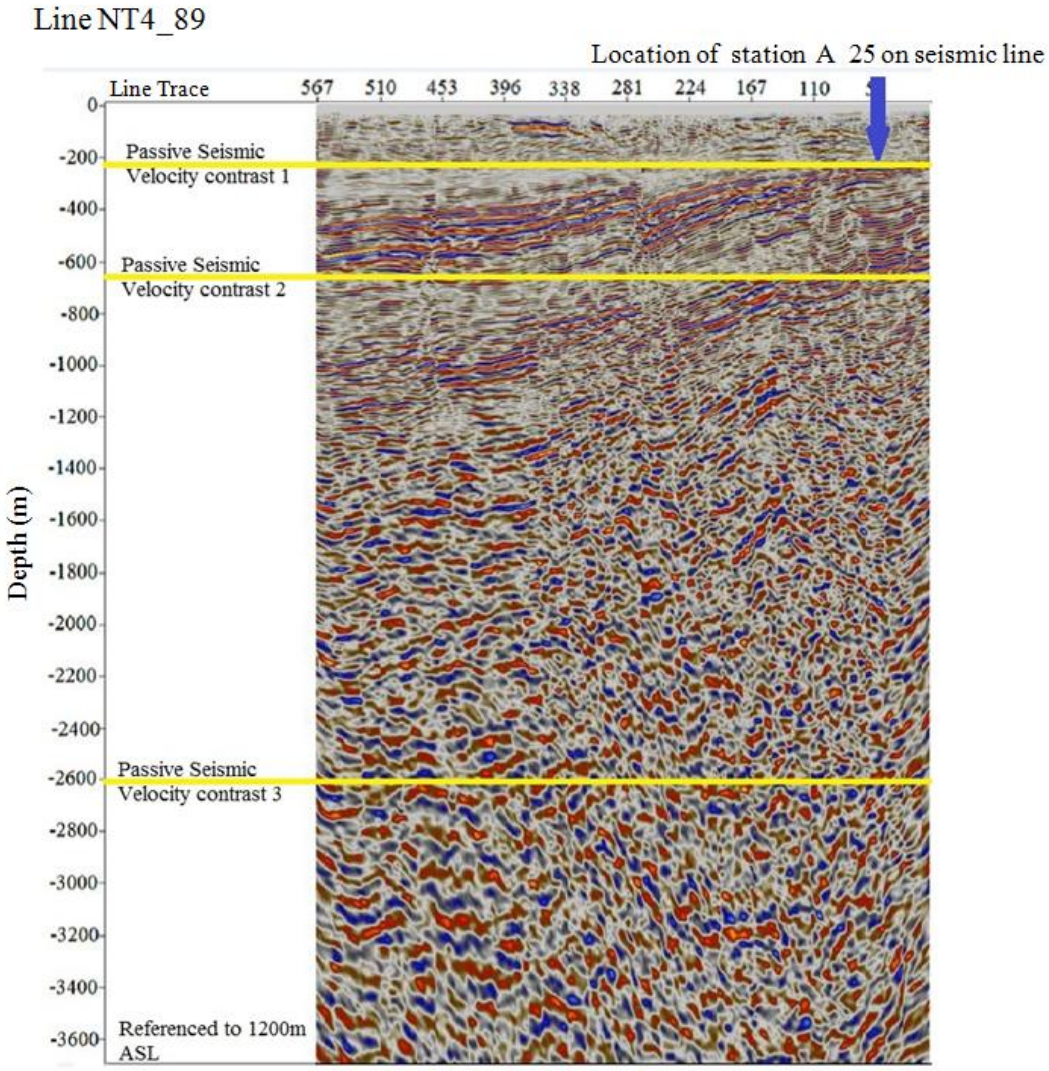


*Figure 5.18(a): Location of station A_25 on seismic line NT4_89. Source: Tullow Oil Ltd*

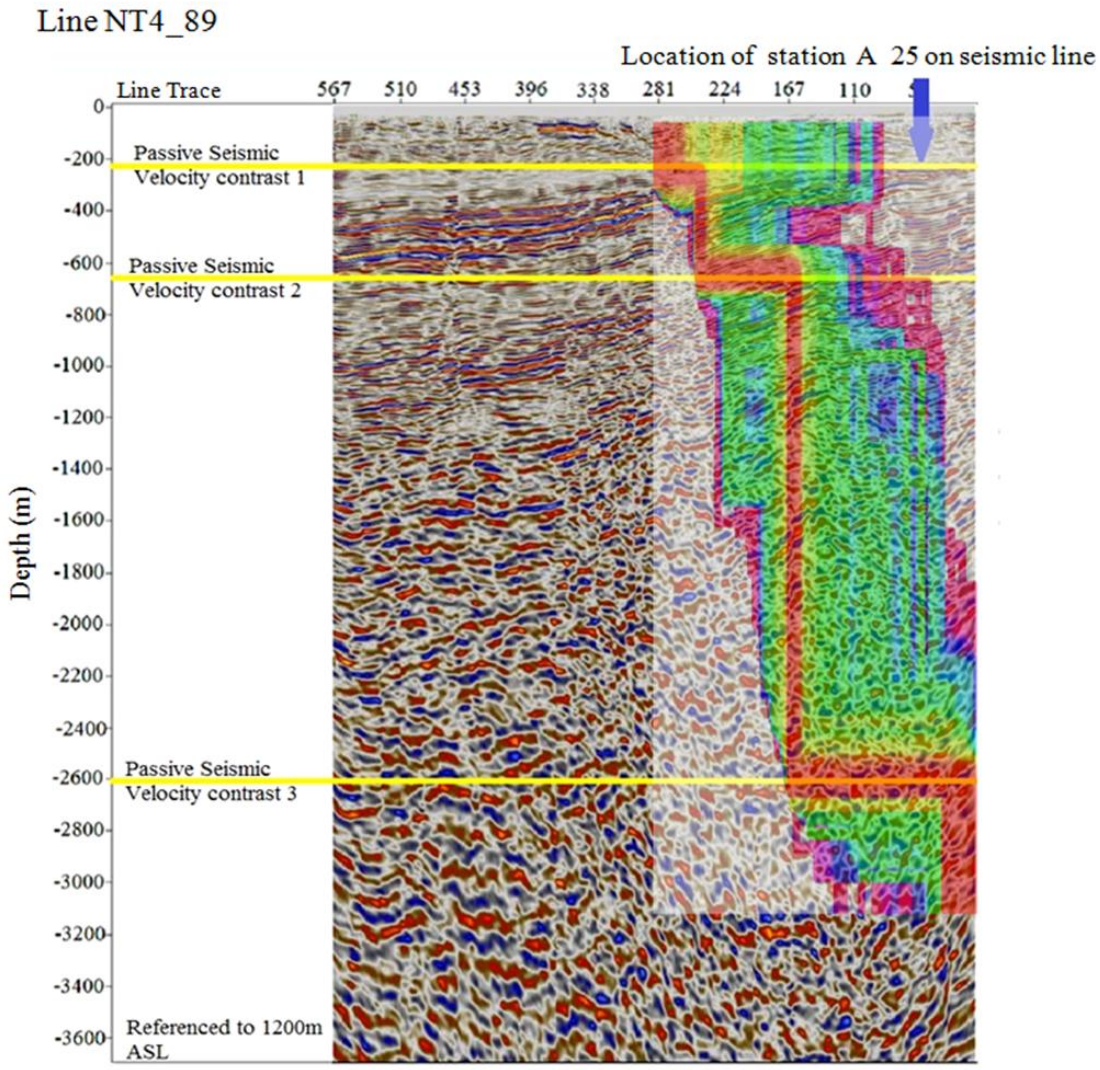


*Figure 5.18(b): Comparison of 2D active seismic data from line NT4_89 with passive seismic velocity model from station A_25. Source: Tullow Oil Ltd*

At the location of station A_25, the depth of the third velocity contrast could not be matched with confidence against the seismic stack due to lack of coherency of energy. This horizon, however, could clearly be seen on the active seismic to be deeper as more coherence of energy is achieved away from the location of station A_25. This supports the hypothesis that the basin is deeper than highlighted here by the active seismic.

# CHAPTER 6: DISCUSSION

## 6.1 HVSR

The first objective of this research was to provide resonance frequencies of Nyanza basin in Ahero. This was achieved by calculating the horizontal to vertical ratio curves for each station in the array and for the stand alone stations. These curves all showed very similar and stable resonance frequency values, spanning the same frequency range. All curves had a main broad pick at around 0.45Hz followed by narrow picks at higher frequencies. The peaks were slightly variable from station to station but were located within the same frequency range. Stations close to Ahero town and closer to roads tended to have higher frequency values for the secondary peaks (ranging from 3 Hz to 8Hz or more) than those in relatively quiet environments. The secondary peaks for the curves were, therefore, assumed to be as a result of local sources while the first stable peaks for each curve are related to fundamental resonance frequency of the study area. Secondary peaks were not used in the analysis and future work, outside the scope of this dissertation, is needed to constraint the nature and origin of these peaks. The average HVSR for the array was then computed and a single average curve obtained. Frequencies below 0.1 Hz were not considered because of the possibility of the real signature of the wavefield being masked by the instrumental noise (cut off frequency of the instrument is 0.03 Hz though the main energy was recorded above 0.1 Hz in this area).

## 6.2 Frequency Wavenumber (F-K)

The array data analysis was based on a semblance approach following Wathelet (2008) and Wathelet et al. (2008) i.e., for each frequency (f), the energy coherently propagating with wavenumber (k) was stacked. The main assumption of this technique is that waves are planar and travelling horizontally (Capon, 1969).

The dispersion curve was clearly inferred between 0.9 Hz and 2.5 Hz. At low frequencies (below 0.2 Hz), there was no coherent energy seen in the colour scale of the dispersion curve suggesting that the maximum distance between the stations ($D_{max}$) was not sufficient to analyse the corresponding long wavelengths ($\lambda$) because the criterion proposed by Wathelet et al. (2008) that $\lambda < 3\ D_{max}$ was no longer fulfilled (Martini et al., 2013).

### 6.3 Inversion

Inversion was performed in two parts: 1) joint inversion of the array's dispersion curve and average HVSR curve as the input targets and, 2) inversion of the HVSR curves for the stand alone stations outside the array.

This process yielded $V_P$ and $V_S$ velocity models. The $V_S$ velocity model was used to infer velocities of surface waves following Xia et al. (2003). The big velocity changes suggested a change in lithology from one formation to another of different consolidation.

The outputs were all normally dispersive profiles, i.e., they had linearly increasing velocities. All stations had three velocity contrasts where the first contrast was occurring at depths averagely less than 250m. A second interface, as a result of change in lithology, occurred at approximate depths of 550m, 650m and 600m for stations A_16, A_19 and A_25, respectively. A third deeper and bigger velocity contrast occurred at depth estimates of 1200m, 1600m, 1500m and 2600m for the L4 array and stations A_16, A_19 & A_25, respectively, pointing to the possibility of a deeper basin. This, when compared to Saggerson (1952) findings, suggests a transition from Miocene sediments (which are below the Neogene volcanics) deposited during the sub-Miocene peneplain into the Pre-Cambrian rocks or basement. There seemed to be a general increase in basin depth towards the west and south of Ahero town (see figure 4.2) in the regions covered by stand alone stations A_16 and A_25 whereas the L4 array and station A_19 showed a decrease in depth towards the east of Ahero town. More in-depth studies need to be conducted focused on establishing the sub-surface geology of the study area.

### 6.4 Comparison

The first two velocity contrasts highlighted by the passive seismic technique correlated well with the two main bright reflectors of the 2D active seismic stacks above 600m. Passive seismic results highlighted a third deeper reflector as opposed to the active seismic which had little or no coherent energy at depths below 600m, hence no resolution of seismic horizons below this depth.

Station A_25, which was located on the north-east end of the NT4-89 seismic line, showed good correlation with the active seismic data at average depths of 200m and 600m (for the first two interfaces) but also highlighted an even deeper reflector at an approximate depth of 2600m (figure 5.14 (a)) which the 2D seismic stacks didn't resolve with confidence. This is

due to presence of volcanics which caused scattering hence affecting the signal strength and in return resulting in poor or no resolution of sediments beneath it.

A summary of the average depth estimates for the three velocity contrasts obtained in this research together with those of the 2D active seismic were presented in table 6.1.

*Table 6.1: Average depth estimates obtained from passive seismic technique compared to those of active seismic method*

| | Depth (m) | | |
|---|---|---|---|
| | **1st Reflector** | **2nd Reflector** | **3rd Reflector** |
| **L4 Array** | 120 | 550 | 1200 |
| **A-16** | 170 | 550 | 1600 |
| **A-19** | 220 | 650 | 1500 |
| **A-25** | 200 | 600 | 2600 |
| **2-D stacks (Active Seismic)** | 200 | 600 | No coherency |

# CHAPTER 7: CONCLUSION AND RECOMMENDATION

## 7.1 Conclusion

A low impact, cost effective passive method was used to obtain velocity profiles from resonance frequencies and dispersive characteristics of Rayleigh waves of the ambient wavefield. This was achieved by deploying high sensitivity 3-component broadband sensors in both a semi-circular array (L4 array) and stand alone station configurations to record ambient noise in Ahero of the Nyanza Basin in Kisumu County. The recorded data was then processed using two techniques: the HVSR and the F-K to obtain the resonance frequency of the area (a function of sediment thickness) and a dispersion curve (a function of depth of basin) respectively. The outputs of the two techniques were, therefore, HVSR curves and a dispersion curve respectively. The two curves were then inverted to obtain velocity profiles from which the average depth estimates as well as the average thickness estimates were directly read. In the case of the L4 array, a joint inversion of the dispersion curve and averaged HVSR curve was performed and a velocity profile obtained. The first objective of this research was thus achieved.

The velocity profiles obtained from inversion provided information on impedance contrasts between sediments and the bedrock and their respective average depth estimates at which they occurred. The thickness and depth estimates to the basement were thus obtained from the velocity profiles. Basin depths estimated from both the L4 array and stand alone stations suggested a general increase in depth of the basin towards the west and south of Ahero town, the deepest part being around Awach, to the south of Ahero town where station A_25 was located. The passive seismic technique was, therefore, successfully used to provide depth to basement (and subsequently its thickness) estimates of Ahero in the Nyanza basin, Kisumu County, Kenya. The passive seismic results correlated well at relatively shallow depths with those of a 2D active seismic survey carried out in the area in 1989. The resolution of the 2D seismic stacks was, however, poor at greater depths, whereas the passive seismic results highlighted a deeper reflector at those greater depths.

## 7.2 Recommendation

The passive seismic technique shows great potential as a powerful low impact exploration tool. In this research, it was successfully used to provide basin depth estimates in Ahero albeit with challenges. It is, therefore, recommended that prior knowledge of the geological

structure be a prerequisite in processing and analysis of the passive seismic data to prevent misinterpretation of results. A reconnaissance survey to a site prior to carrying out a passive seismic survey would be vital in assessing possible localised noise sources that may contaminate the data in the frequencies of interest.

Introduction of more constraints, e.g., lithology logs/ well logs would give this technique more confidence in picking out the various specific formations characterizing a basin. This method has been mostly used in soil characterization in geotechnical engineering without much focus on the identification of various formations encountered. The possibility of incorporating shear slowness to lithology identification in the passive seismic data processing techniques may provide a more robust and effective platform for exploration.

## REFERENCES


Aki, K. (1957). Space and time spectra of stationary stochastic waves, with special reference to microtremors. *Bulletin of the Earthquake Research Institute, University of Tokyo*, 35, pp.415-457.

Aki, K. (1965). A note on the use of microseisms in determining the shallow structures of the earth's crust. *Geophysics*, 30, pp.665-666.

Aki, K. and Richards, P. (2002). *Quantitative seismology*. 2nd ed. University Science Books.

Arai, H. (2004). S-Wave Velocity Profiling by Inversion of Microtremor H/V Spectrum. *Bulletin of the Seismological Society of America*, 94(1), pp.53-63.

Arai, H. (2005). S-Wave Velocity Profiling by Joint Inversion of Microtremor Dispersion Curve and Horizontal-to-Vertical (H/V) Spectrum. *Bulletin of the Seismological Society of America*, 95(5), pp.1766-1778.

Asten, M. (1978). Geological control of the three-component spectra of Rayleigh-wave microseisms. *Bulletin of the Seismological Society of America*, 68, pp.1623-1636.

Asten, M. and Henstridge, J. (1984). Array estimators and the use of microseisms for reconnaissance of sedimentary basins. *Geophysics*, 49(11), pp.1828-1837.

Banerji, S. (1924). Microseisms associated with the Incidence of the South-west Monsoon. *Nature*, 114(2868), pp.576-576.

Bard, P. (1998). Microtremor measurements: A tool for site effect estimation? In: *2nd International Symposium on The Effects of Surface Geology on Seismic Motion*. Balkema, pp.1251-1279.

Bolt, B. (1978). Earthquakes Hazards. *American Geophysical Union*, 59(11), pp.946.

Bonnefoy-Claudet, S., Cornou, C., Bard, P., Cotton, F., Moczo, P., Kristek, J. and Fäh, D. (2006). H/V ratio: a tool for site effects evaluation. Results from 1-D noise simulations. *Geophysical Journal International*, 167(2), pp.827-837.

Bonnefoy-Claudet, S., Cotton, F. and Bard, P. (2006). The nature of noise wavefield and its applications for site effects studies. *Earth Science Reviews*, 79(3-4), pp.205-227.

Bourbié, T., Coussy, O. and Zinszner, B. (1987). Acoustics of Porous Media. Gulf Publishing Company, Book Division, pp.176-339.

Capon, J. (1969). High-resolution frequency-wavenumber spectrum analysis. *Proceedings of the IEEE*, 57(8), pp.1408-1418.

Delgado, J., Casado, C., Giner, J., Estevez, A., Cuenca, A. and Molina, S. (2000). Microtremors as a geophysical exploration tool: applications and limitations. *Pure and Applied Geophysics*, 157(9), pp.1445-1462.

Foti, S. (2000). Multistation Methods for Geotechnical Characterization using Surface Waves. PhD. Politecnico di Torino.

Foti, S., Lai, C., Rix, G. and Strobbia, C. (2014). Surface wave methods for near-surface site characterization. CRC Press.

Gu'eguen, P., Cornou, C., Garambois, S. and Banton, J. (2007). On the limitation of the H/V spectral ratio using seismic noise as an exploration tool: application to the Grenoble valley (France), a small apex ratio basin. *Pure and Applied Geophysics*, 164(1), pp.115-134.

Hobiger, M., Le Bihan, N., Cornou, C. and Bard, P. (2012). Multicomponent Signal Processing for Rayleigh Wave Ellipticity Estimation: Application to Seismic Hazard Assessment. *IEEE Signal Process Magazine*, 29(3), pp.29-39.

Ichang'i, D. and MacLean, W. (1991). The Archean volcanic facies in the Migori segment, Nyanza greenstone belt, Kenya: stratigraphy, geochemistry and mineralisation. *Journal of African Earth Sciences (and the Middle East)*, 13(3-4), pp.277-290.

Ibs-von Seht, M. and Wohlenberg, J. (1999). Microtremor measurements used to map thickness of soft sediments. *Bulletin of the Seismological Society of America*, 89(1), pp.250-259.

Kent, P. (1944). The Miocene beds of Kavirondo, Kenya. *Quarterly Journal of the Geological Society*, 100(1-4), pp.85-118.

Kudo, K. (1995). Practical estimates of site response. State-of-art report. In: *Proceedings of the fifth International Conference on Seismic Zonation*. Nice, France.

Lachet, C. and Bard, P. (1994). Numerical and Theoretical Investigations on the Possibilities and Limitations of Nakamura's Technique. *Journal of Physics of the Earth*, 42, pp.377-397.

Martini, F., Davi, R., Doherty, J. and Mongan, J. (2015). Ambient noise to estimate depth to basement: case studies from East Africa basins. *First Break*, 33(2056).

Martini, F., Lokmer, I., Jonsdottir, K., De Barros, L., Möllhoff, M., Bean, C., Hauser, F., Doherty, J., Ryan, C. and Mongan, J. (2013). A passive low-frequency seismic experiment in the Albertine Graben, Uganda. *Geophysical Prospecting*, 61, pp.39-61.

Menke, W. (1989). *Geophysical data analysis*. San Diego: Academic Press.

Nakamura, Y. (1989). A method for dynamic characteristics estimation of subsurface using microtremor on the ground surface. *Railway Technical Research Institute, Quarterly Reports*, 30(1).

Nogoshi, M. and Igarashi, T. (1970). On the propagation characteristics of microtremors. *Journal of the Seismological Society of Japan*, 23, pp.264-280.

Novotný, O., Burlako, L. and Proskuryakova, T. (1996). Modifications of the dispersion relations for surface waves in a layer on a half-space. *Studia Geophysica Geodaetica*, 40(2), pp.167-177.

Parolai, S., Picozzi, M., Richwalski, S. and Milkereit, C. (2005). Joint inversion of phase velocity dispersion and H/V ratio curves from seismic noise recordings using a genetic algorithm, considering higher modes. *Geophysical research letters*, 32(1).

Picozzi, M., Parolai, S. and Richwalski, S. (2005). Joint inversion of H/V ratios and dispersion curves from seismic noise: Estimating the S-wave velocity of bedrock. *Geophysical Research Letters*, 32(11).

Pulfrey, W. (1946). *Geological survey of Maragoli, Northern Kavirondo*. Report (Geological Survey of Kenya) number 9. Government Printer, Nairobi.

Reynolds, J. (1997). An Introduction to Applied and Environmental Geophysics. John Wiley and Sons Ltd, Chichester.

Saggerson, E. (1952). *Geology of Kisumu District*. Report (Geological Survey of Kenya)

Issue 21. Government Printer, South Africa.

Salop, L. (1983). Geological evolution of the earth during the Precambrian. *Berlin: Springer-Verlag.*

Sambridge, M. (1999). Geophysical inversion with a neighbourhood algorithm: Searching a parameter space. *Geophysical Journal International*, 138(2), pp.479-494.

Sambridge, M. and Drijkoningen, G. (1992). Genetic algorithms in seismic waveform inversion. *Geophysical Journal International*, 109(2), pp.323-342.

Tokimatsu, K. (1997). Geothermal site characterization using surface waves. *Earthquake Geotechnical Engineering*, K. Ishihara (Editor), Balkema, Rotterdam, 1333-1368.

Tokimatsu, K., Shinzawa, K. and Kuwayama, S. (1992). Use of Short-Period Microtremors for Vs Profiling. *Journal of Geotechnical Engineering*, 118(10), pp.1544-1558.

Wathelet, M., Jongmans, D. and Ohrnberger, M. (2004). Surface-wave inversion using a direct search algorithm and its application to ambient vibration measurements. *Near surface geophysics*, 2(4), pp.211-221.

Wathelet, M., Jongmans, D. and Ohrnberger, M. (2005). Direct inversion of spatial autocorrelation curves with the neighbourhood algorithm. *Bulletin of the Seismological Society of America*, 95(5), pp.1787-1800.

Xia, J., Miller, R., Park, C. and Tian, G. (2003). Inversion of high frequency surface waves with fundamental and higher modes. *Journal of Applied Geophysics*, 52(1), pp.45-57.

Yilmaz, Ö. (2015). Engineering Seismology with Applications to Geotechnical Engineering. *International Society of Applied Geophysics,* Series No. 27. Society of Exploration Geophysicists, pp.67-145.

Zhang, S. and Chan, L. (2003). Possible effects of misidentified mode number on Rayleigh wave inversion. *Journal of Applied Geophysics*, 53(1), pp.17-29.

## APPENDICES

The HVSR curves from the remaining L4 array stations are given below. An amplified geological map (Figure 2.3) is also provided:

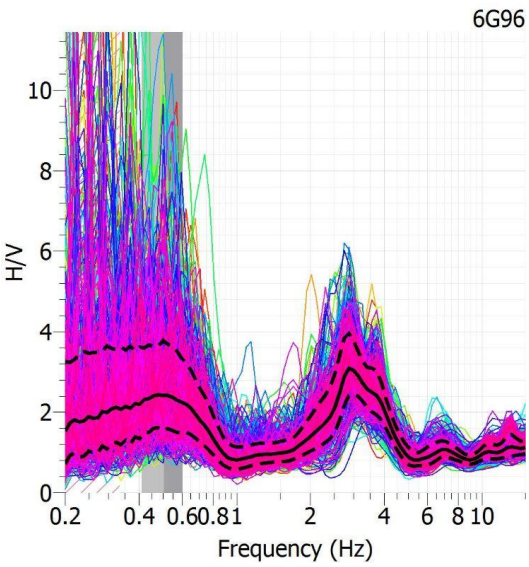


Station L04_01

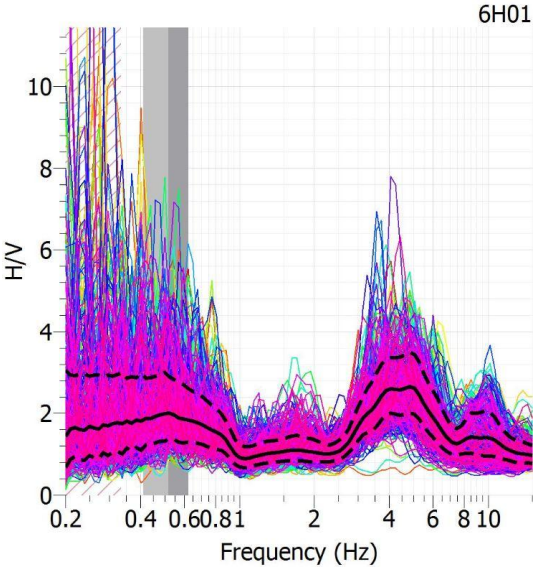


Station L04_02

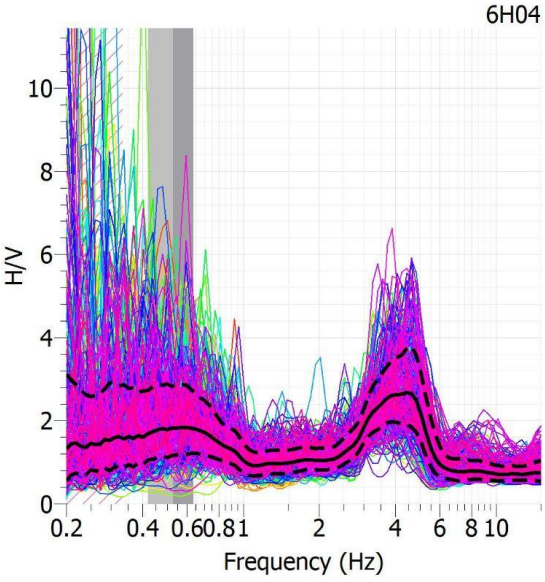


Station L04_03

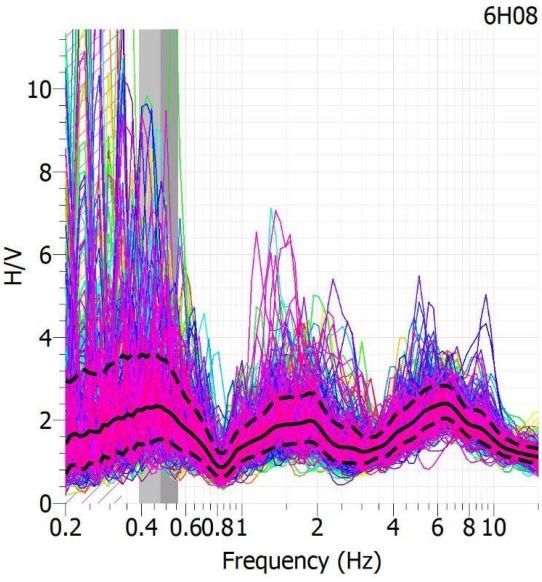


Station L04_04

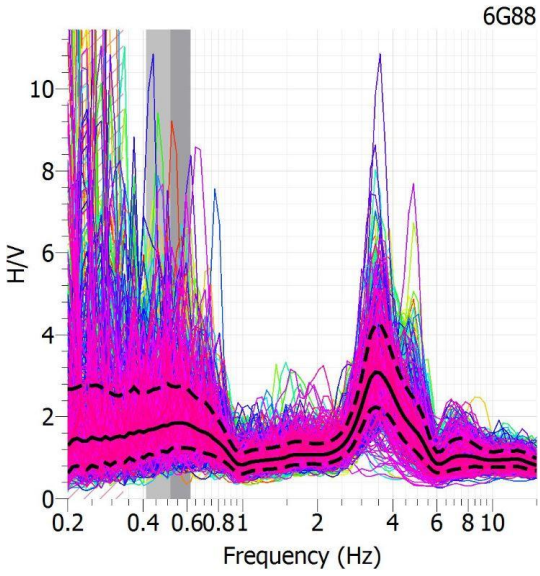


Station L04_05

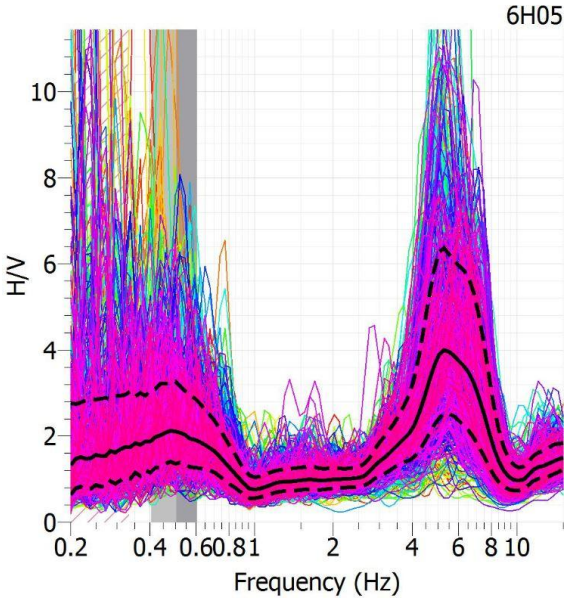


Station L04_06

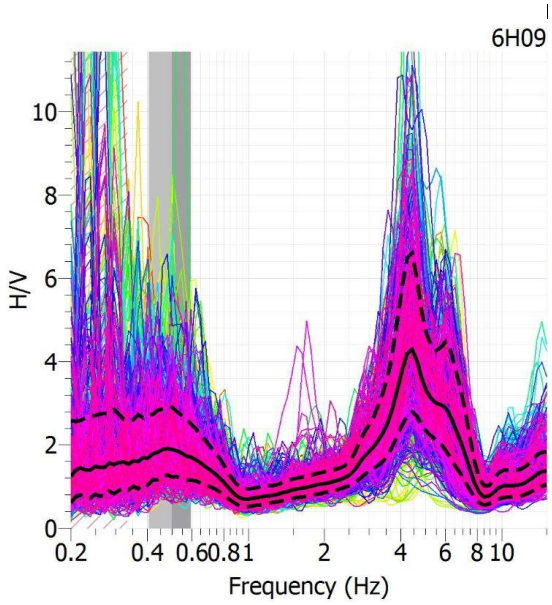


Station L04_08

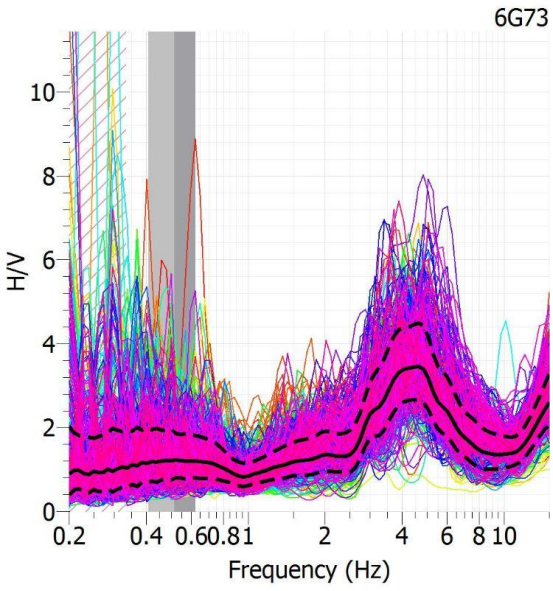


Station L04_09

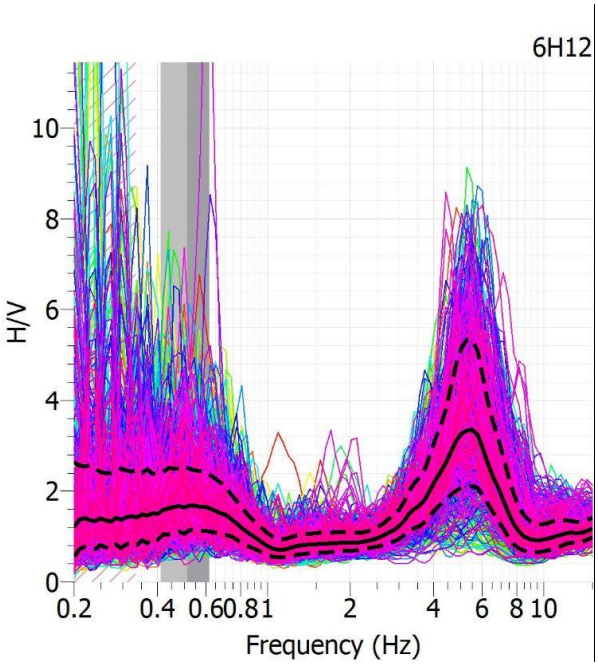


Station L04_10

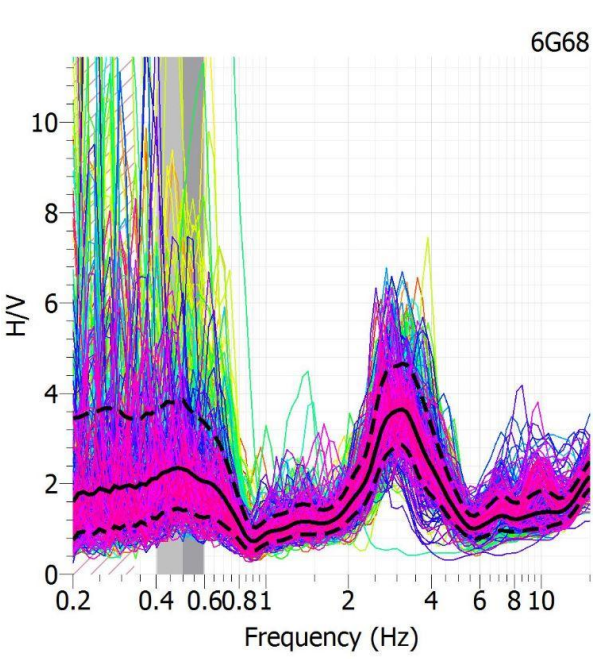


Station L04_12

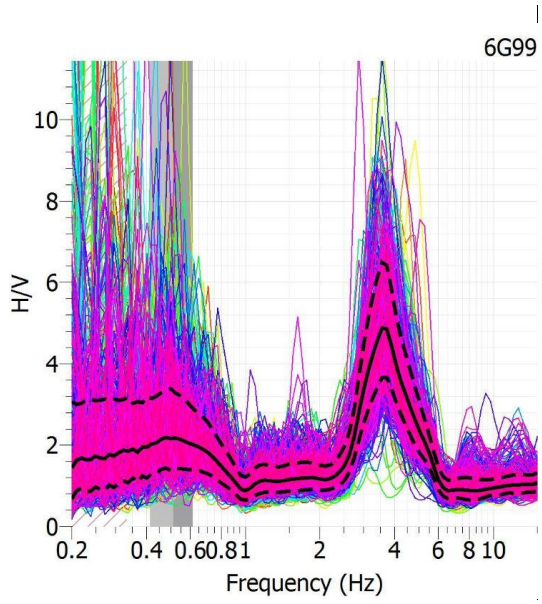


Station L04_14

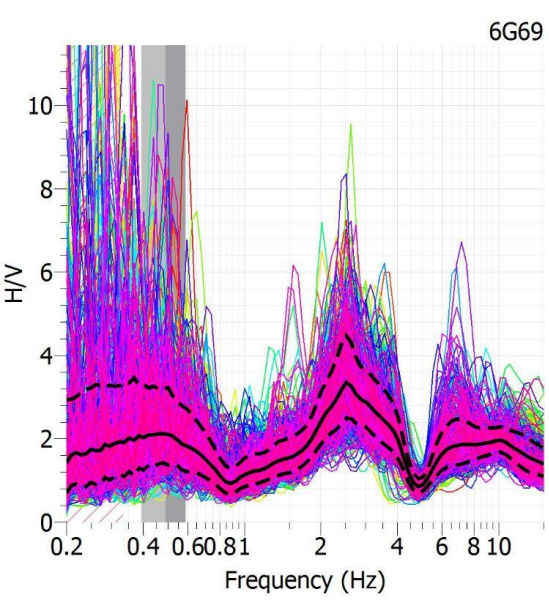


Station L04_15

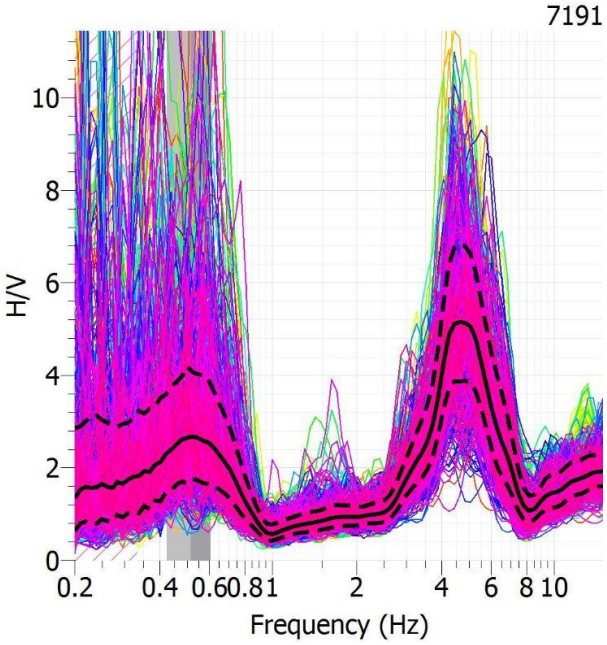


Station L04_16

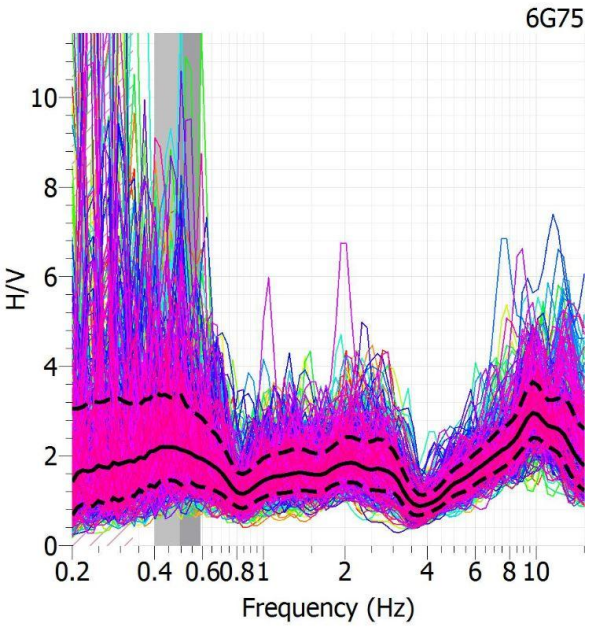


Station L04_17

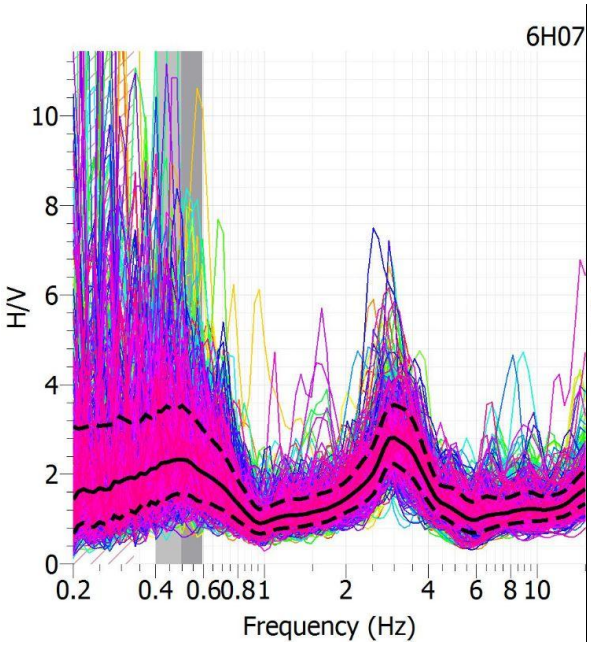


Station L04_19

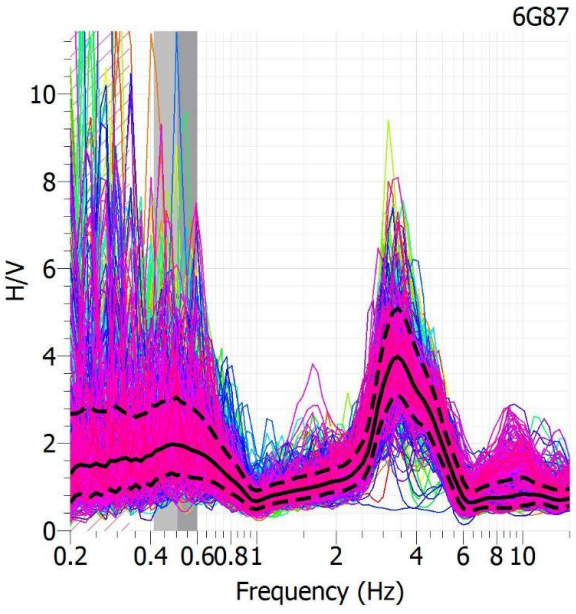


Station L04_20

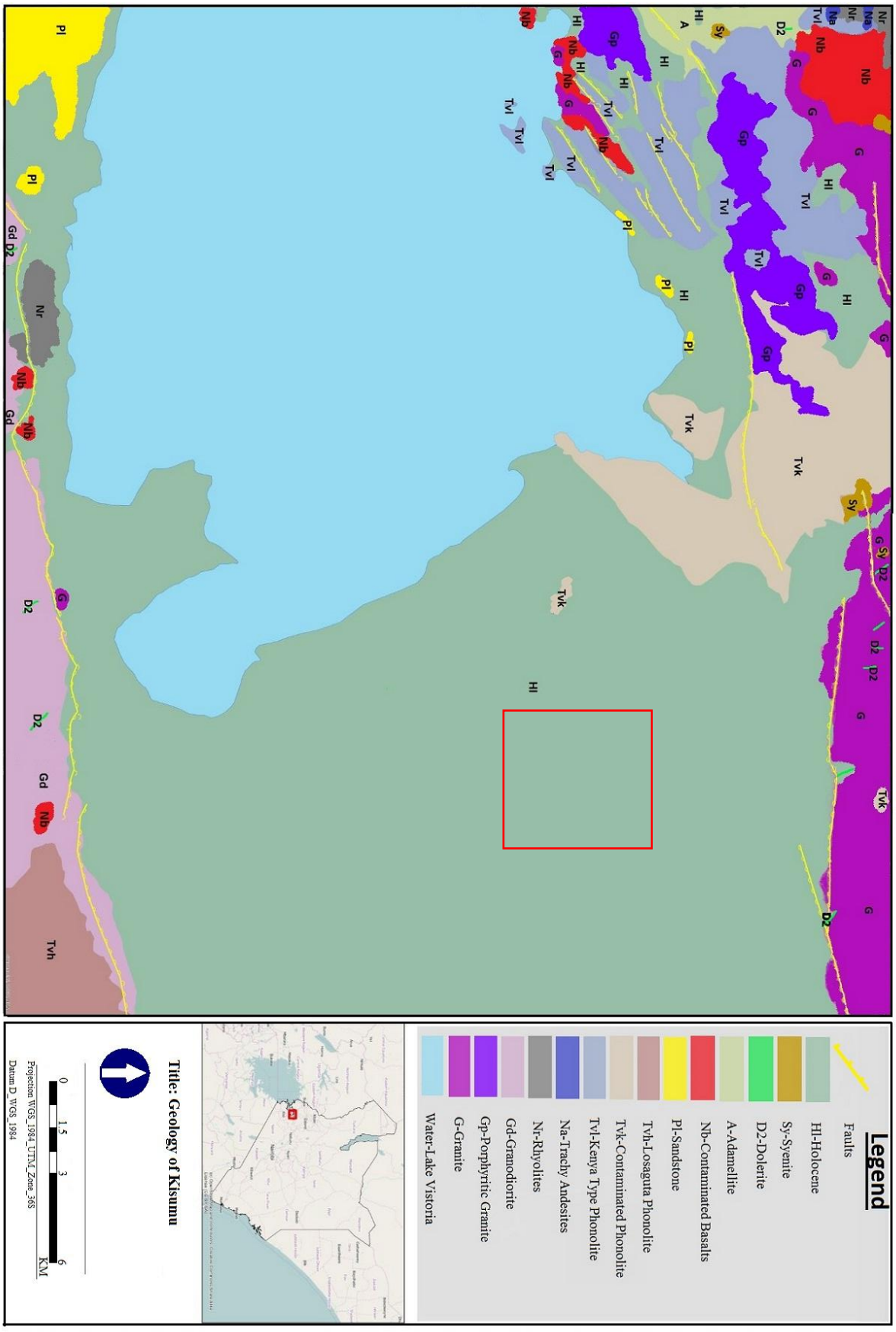


*Figure 2.3: Geological map of Kisumu region. The red box represents the area covered by this research. The yellow lines represent faults in this region. Adopted from Saggerson, (1952)*